Acta Geochim (2025) 44:1254–1275
https://doi.org/10.1007/s11631-025-00776-9

ORIGINAL ARTICLE

Extraction of deep mineralization information from weak and low tectono-geochemical anomalies: A case study of the Maoping germanium-rich lead–zinc deposit in northeastern Yunnan Province, China

Yixuan Yang[1] · Gaoming Zhou[2] · Runsheng Han[1] · Hongsheng Gong[1] · Jianbiao Wu[1] · Yan Zhang[1] · Yaya Mi[1]

Received: 2 January 2025 / Revised: 18 March 2025 / Accepted: 18 March 2025 / Published online: 19 May 2025

Abstract Tectono-geochemical analysis is one of the key technical methods for deep prospecting and prediction, but the extraction of information on weak and low degrees of mineralization remains a significant challenge. This study takes the Maoping super-large germanium-rich lead–zinc deposit in northeastern Yunnan as an example, systematically analyzes the mineralization element assemblages and their anomaly distribution characteristics, extracts information on low and weak anomalies at depth, clarifies the spatial distribution of ore-forming element anomalies and fluid migration patterns, and establishes tectono-geochemical deep anomaly evaluation criteria and prospecting models, thereby proposing directions for deep prospecting in the deposit. This research shows that the mineralization element assemblage of the F1 factor (Cd-Cu-Ge-Zn-Sb-In-Pb-Sr(-)-As-Hg) anomalies represents near-ore halos; the element assemblage of the F2 factor (Ni-Co-Cr-Rb-Ga) anomalies represents tail halos; the element assemblage of the F3 factor (Rb-Mo-Tl-As) anomalies represents front halos; and the element assemblage of the F4 factor (Ba-Ga) anomalies represents barite alteration anomalies. Elements such as Zn and Pb exhibit significant anomalies near the lead–zinc ore bodies. In the study area, vertical anomalies in the eastern region of the Luoze River indicate that ore-forming fluids migrated from the SE at depth to the NW at shallower levels, whereas in the western region, ore-forming fluids migrated from the SW at depth to the NE at shallower levels. Thus, the lateral extensions of different ore bodies in the eastern and western regions of the river have been determined. On this basis, tectono-geochemical deep anomaly evaluation criteria for the deposit are established, and directions for deep prospecting are proposed. This study provides scientific value and practical significance for deep prospecting and exploration engineering planning for similar lead–zinc deposits.

Keywords Tectono-geochemistry · Element association · Maoping germanium-rich lead-zinc deposit · Extraction of deep mineralization information · Anomaly evaluation index

1 Introduction

Tectono-geochemistry is the study of the relationships between tectonic processes and the distribution, migration, dispersion, and enrichment of chemical elements in the Earth's crust. On the one hand, it investigates the geochemical processes involved in tectonic activities; on the other hand, it examines the tectonic processes that are caused by and reflected in geochemical processes (Tu 1984). The practical significance of tectono-geochemistry lies in studying the movement of elements in the Earth's crust and their distribution patterns both temporally and spatially, thereby revealing their relationships with the development of crustal tectonics. This helps clarify the migration and enrichment patterns of ore-forming elements, providing an important theoretical foundation for mineral exploration and ore formation prediction. This is especially significant for the prediction and identification of deep and peripheral concealed

Gaoming Zhou, Hongsheng Gong, Jianbiao Wu, Yan Zhang, Yaya Mi have contributed equally to this work.

✉ Runsheng Han
11301124@kust.edu.cn

[1] Land Resource Engineering, Kunming University of Science and Technology, South-West Institute of Geological Survey, Geological Survey Center for Nonferrous Metals Resources, Kunming 650093, China

[2] Yiliang Chihong Co., Ltd, Zhaotong 657600, Yunnan, China

ores in old mines that are clearly controlled by tectonics (Han et al. 2015). Tectono-geochemical exploration techniques play crucial roles in identifying mineral deposits that are tectonically controlled (Gong et al. 2021; Wan et al. 2022). Han et al. (2015) proposed the method of finding ore deposits through identifying anomalies in metal element assemblages in fault-controlled rock (MEAHFZ), as anomalies in mineralization-related element combinations effectively provide prospecting information for deep concealed ore bodies and can accurately determine the specific location and extension direction of deep concealed ore bodies (Han 2013; Cheng et al. 2024).

Low–weak geochemical anomalies refer to subtle anomalies in complex geological settings, where the overlapping of multiple geological units above the ore body makes it difficult to identify mineralization information (Fan et al. 2024). Given the dual background of practical application requirements and the support of vast amounts of data, the development of geochemical anomaly identification and extraction techniques under complex geological conditions is particularly important. This involves the mining and redevelopment of exploration geochemical data, subsequently extracting geochemical ore-related anomalies to drive breakthroughs in mineral exploration (Zuo 2019). However, the extraction of mineralization information from low–weak tectono-geochemical anomalies remains a key challenge in deep mineral exploration. Therefore, it is necessary to study such anomalous information, clarify the multi-scale spatial variation characteristics of geochemical elements, and then propose mineral exploration directions in order to provide a scientific basis for the exploration of deep and peripheral parts of hydrothermal ore deposits.

Domestic and international research efforts in recent years have yielded numerous innovative theories and methodologies for mineral deposit studies and prospecting prediction, including the similarity analogy theory, geological anomaly metallogenic theory, geological condition assemblage ore-controlling theory (Zhao and Chen 1998), metallogenic series theory (Chen 1994), comprehensive information evaluation theory (Wang et al. 1992), metallogenic system theory (Zhai 1999), "trinity" mineral resource prediction and evaluation theory (Zhao et al. 2022), GIS-based mineral prediction (Xiao et al. 2000), structural metallogenic dynamics (Han 2003), integrated geological information prediction technology for solid mineral deposits (Ye et al. 2007), "three-stage" mineral resource assessment methodology (Xiao et al. 2006), ore field (deposit) structural geochemistry (Han et al. 2015), and tectono-lithofacies and geochemical lithofacies analysis (Fang 2016).

Recent technological advancements have driven the transformation of deep mineral exploration technologies toward high-tech applications, including 3D visualization and data modeling (Wang et al. 2021), big data and machine learning approaches (Ghezelbash et al. 2019), numerical simulation techniques (Chelle-Michou et al. 2017), high-resolution aerial and satellite remote sensing technologies (Bauer et al. 2022), and deep drilling technologies (Speczik et al. 2021). Significant progress has also been made in deep electromagnetic detection, 3D seismic surveys, and airborne geophysical exploration (Yang et al. 2020). These theoretical and methodological developments have provided effective guidance for mineral prospecting prediction.

However, conventional geochemical single-element analysis has insufficient sensitivity to low-intensity anomalies in complex tectonic settings and struggles to differentiate mineralization factors from non-mineralization factors. To address these technical challenges, this study proposes an innovative approach: through the integration of multivariate statistical analysis, we establish mapping relationships between element assemblages and geological processes, construct element covariance matrices, and systematically analyze the spatial correlations of elemental associations. This methodology effectively compensates for existing technological limitations, significantly enhances the identification of mineralized anomalies in complex geological environments, and provides novel insights for concealed ore deposit prediction.

The Sichuan–Yunnan–Guizhou border region is located in the transitional zone between the Tethyan metallogenic domain and the circum-Pacific metallogenic domain, where carbonate-hosted, non-magmatic, epigenetic, hydrothermal-type Pb–Zn deposits (CNHTs) are widely distributed. The germanium-rich lead–zinc deposits in this region are defined as HZT deposits. They occur in an intracontinental strike-slip or collisional orogenic tectonic setting, with fault–fold structures and rock assemblages being the main factors controlling mineralization (Han et al. 2020, 2022; Wu et al. 2024b). Among them, the Maoping superlarge germanium-rich lead–zinc deposit in northeastern Yunnan is a typical representative of this type of deposit. The Maoping mining area is located in the core of the Wumeng Mountains, where the terrain is high and steep, with deep ore bodies and weak surface tectono-geochemical anomalies. Extracting mineralization information on concealed ore bodies has become one of the key challenges in deep mineral exploration. Currently, significant progress has been made in research on the Maoping lead–zinc deposit, particularly in the areas of tectono-geochemical studies and the prediction of concealed ore bodies, yielding good exploration results. For example, experts and scholars such as Han et al. (2010), Wang (2010), and Chen (2014) have conducted detailed tectono-geochemical studies and predictions of concealed ore bodies in sections at 910, 846, 814, 760, and 670 m, and other depths.

The Maoping Ge-rich Pb–Zn deposit is structurally controlled by an oblique thrust strike-slip and fault–fold system (Han et al. 2019). The NE-striking Fangmaba Fault,

Maoping Fault, and Daibu Fault, which are arranged in an imbricate pattern, combined with their hanging wall-derived anticlines, collectively govern the distribution of the Maoping Pb–Zn ore field. Specifically, the Maoping Fault and its associated Maomaoshan anticline constitute an oblique thrust strike-slip and fault–fold system that controls the location of the Ge-enriched Pb–Zn deposit. Ore bodies occur predominantly within NE–SW-trending interlayer fracture zones, with secondary faults and joint–fracture zones controlling vein distribution. The structural evolution of the mining area has involved four developmental stages, namely, N–S-trending → NE–SW-trending → NW–SE-trending → E–W-trending structural zones, among which the NE–SW-trending structural zone constitutes the metallogenic structural system (Wu et al. 2023).

Previous attempts to determine the metallogenic age of the Maoping deposit yielded divergent results. Yang et al. (2019) obtained a Rb–Sr isochron age of 202.5 ± 8.5 Ma from sphalerite. Shen et al. (2016) reported a sphalerite Rb–Sr isotope age of 321.7 ± 5.8 Ma (MSWD = 1.5) for the Ge-rich Pb–Zn deposit. Ji (2019) identified two concordant zircon U–Pb ages of 448 ± 4 Ma (MSWD = 0.85) and 305 ± 3 Ma (MSWD = 0.64). These results indicate ongoing controversies regarding the metallogenic chronology of the Maoping deposit.

During the metallogenic process of the Maoping Pb–Zn deposit, the structural-fluid coupling exhibits remarkable spatiotemporal differentiation characteristics. The deep-seated ore-forming fluids in the mining area migrated along the SW-NE direction, driven by NE-trending structures and permeated along SE-NW-oriented interlayer structures. During their upward migration from deep to shallow levels, these ore-forming fluids evolved with progressively decreasing temperature, pressure, and salinity but increasing density. Metal sulfide precipitation was ultimately triggered by decompression boiling, water–rock interactions, and mixing with basinal reducing fluids (Wu et al. 2024a). The metallogenic metal-bearing fluids migrated along the ore-conducting structure (Maoping Fault) from the deep SE region to the shallow NW zone, subsequently entering the ore-distributing structural system composed of NNW-trending dextral transtensional fractures and S–N-trending sinistral shear fractures. These fluids preferentially selected the D3zg formation as the primary ore-hosting space before ultimately expanding into the C2w formation (Li 2022).

However, the following issues remain in the current mining area: (1) Current tectono-geochemical studies are focused mostly on the distribution of planar anomalies, whereas profile anomaly studies are relatively rare. This not only limits a comprehensive understanding of the spatial structure of ore bodies but also restricts the scientific prediction of deep resource potential. (2) The tectono-geochemical anomaly structure below 670 m in the mining area is still unclear, leading to a lack of precise guidance for deep mineral exploration and affecting the efficiency of resource exploration. (3) The deep extension pattern of the controlling structures and their relationship with the distribution of concealed ore bodies in the deposit have not yet been clarified, which restricts the scientific assessment of deep resource potential. How to efficiently extract mineralization information for concealed ore bodies under complex topographic conditions is a key scientific issue for advancing deep mineral exploration and improving resource exploration efficiency. This is crucial for helping mining enterprises achieve their goals of increasing reserves and production.

Therefore, this study takes the Maoping super-large germanium-rich lead–zinc deposit as a typical example. On the basis of tectono-geochemical theories and methods (Han et al. 2015; Han 2005) and deep underground drilling projects in the mine, this study systematically analyzes the mineralization element assemblages and their anomalous distribution characteristics in different parts and elevations of the deposit. It extracts low–weak tectono-geochemical anomaly information from deep sections of the deposit, clarifies the spatial distribution of mineralization elements and fluid migration patterns, establishes deep anomaly evaluation criteria and a prospecting model for the deposit, and delineates deep prospecting target areas in the mining region. This provides a scientific basis for deep and peripheral exploration predictions of this type of lead–zinc deposit.

2 Metallogenic geological background

The Maoping germanium-rich lead–zinc deposit is a typical super-large CNHT germanium-rich lead–zinc deposit in the lead–zinc polymetallic metallogenic area of the southwestern margin of the Yangtze block. It is located at the intersection of the NE–SW-trending Huize–Niujie oblique strike-slip fault–fold belt, the N–S-trending Qujing–Zhaotong concealed fault zone, and the NW–SE-trending Ziyun–Yadu deep fault zone (Fig. 1) (Han et al. 2019; Wu et al. 2023). On the basis of the Theory and Methods of Geomechanics in Ore Fields (Sun and Han 2015), the deposit is primarily controlled by the NE–SW-trending Maoping compressive shear fault and its hanging wall, as well as the overturned Maomaoshan anticline (Fig. 1). The main structures in the mining area are NE–SW-, NW–SE-, and N–S-trending, with the NE–SW-trending interlayer left-lateral compressive shear fault zone being dominant (Fig. 2). The region features mainly Devonian, Carboniferous, and Permian carbonate–clastic rock sequences, which are predominantly characterized by parallel unconformities and conformable contact relationships. The ore bodies are mainly hosted in the Upper Devonian Zaige Formation (D_3zg) with gray-white to dark gray fine- to medium-grained dolomite, the lower

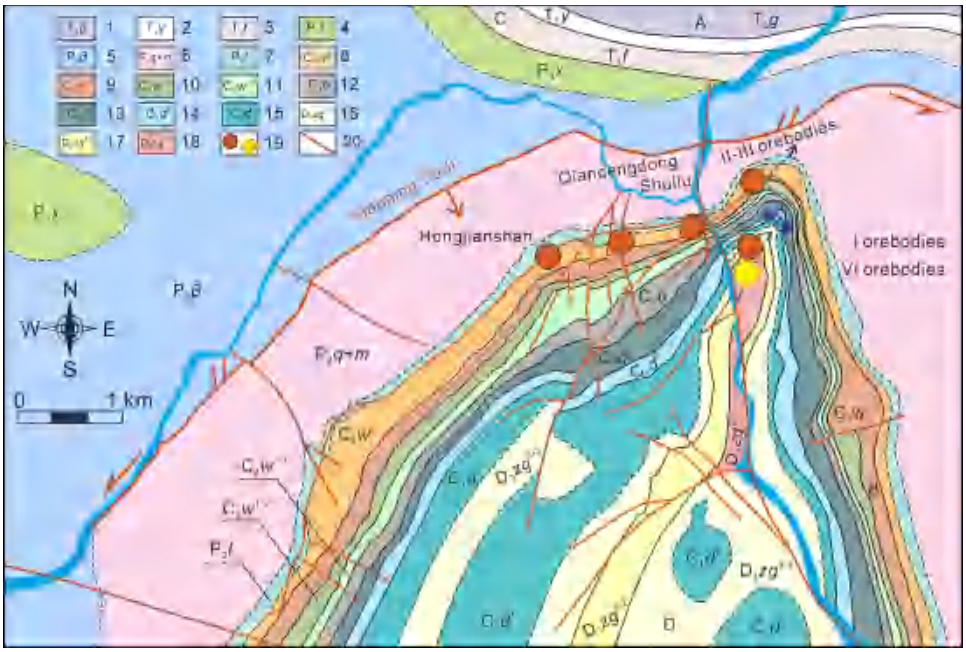

Fig. 1 Geological map of the Maoping Pb–Zn ore field and deposit (Wu et al. 2024a**,** Mine data). 1. Middle Triassic Guanling Formation; 2. Lower Triassic Yongningzhen Formation; 3. Lower Triassic Feixianguan Formation; 4. Upper Permian Xuanwei Formation; 5. Upper Permian Basalt Formation; 6. Middle Permian Qixia + Maokou Formations; 7. Lower Permian Liangshan Formation; 8. Upper Carboniferous Weining Formation; 9. Upper Carboniferous Weining Formation, First Member, Third Submember; 10. Upper Carboniferous Weining Formation, First Member, Second Submember; 11. Upper Carboniferous Weining Formation, First Member, First Submember; 12. Lower Carboniferous Baizuo Formation; 13. Lower Carboniferous Datang Formation, Third Member; 14. Lower Carboniferous Datang Formation, Second Member; 15. Lower Carboniferous Datang Formation, First Member; 16. Upper Devonian Zaige Formation, Third Member, Third Submember; 17. Upper Devonian Zaige Formation, Third Member, Second Submember; 18. Upper Devonian Zaige Formation, Third Member, First Submember; 19. Ore body groups; 20. Faults

Carboniferous Baizuo Formation (C_1b) with light reddish-gray to gray-white massive dolomitic fine-grained limestone, and the upper Carboniferous Weining Formation (C_2w) with light gray to dark gray medium- to thick-bedded dolomitic limestone (Fig. 1). The magmatic rocks are primarily basalts from the upper Permian. The deposit is composed of the no. I, II, III, and VI ore bodies in the ore belt east of the Luoze River and the Shuilu, Qiancengdong, and Hongjianshan ore belts west of the Luoze River. The ore bodies are distributed within the NE–SW-trending interlayer fault zone on the northwestern flank of the overturned Maomaoshan anticline and are lenticular, vein-like, and quasi-stratiform in shape, with a NE-SW orientation. The Hedong mining section is located on the southeast-dipping overturned wing of the Maomaoshan anticline, where the ore body groups, controlled by NE–SW-trending compressive shear faults within different stratigraphic units, exhibit a left-lateral distribution in plan view. In contrast, the Hexi mining section is located on the northwest-dipping non-overturned wing of the Maomaoshan anticline, where the ore body groups, controlled by compressive shear fault zones, show a right-lateral distribution in plan view (Fig. 2) (Han et al. 2024). The ore bodies are mainly lenticular, vein-like, and stratiform-like. The main ore minerals include galena, sphalerite, and pyrite, and the gangue minerals include dolomite, calcite, a small amount of quartz, and barite. The ore structures are compact massive disseminated, vein-like, veinlet-like, massive and stellate, and the ore textures are mainly granular and metasomatic. The main types of wall rock alteration include pyritization, ferritization, dolomitization, calcification, and silicification (Wu et al. 2024b).

The deposit consists of the I, II, III, and VI ore body groups east of the Luoze River (Hedong mining section) and the Shuilu, Qiancedong, and Hongjianshan mining sections west of the Luoze River (Hexi mining section). The I ore body group is located within the interlayer fault zone of the D_3zg^{3-2} Formation, with a NE–SW strike, SE dip, and dip angles ranging from 60° to 85°. The II and III ore body groups are located within the interlayer fault zones of the C_1b Formation and the C_2w^{1-2} Formation, with a NE–SW strike, SE dip, and dip angles ranging from 60° to 90°. The VI ore body group is situated within the interlayer fault zone of the D_3zg^{3-1} Formation, with a NE–SW strike, SE dip, and dip angles ranging from 50° to 70°. The ore bodies in the Shuilu, Qiancedong, and Hongjianshan mining sections are all located within the interlayer fault zone of the C_2w^{1-2}

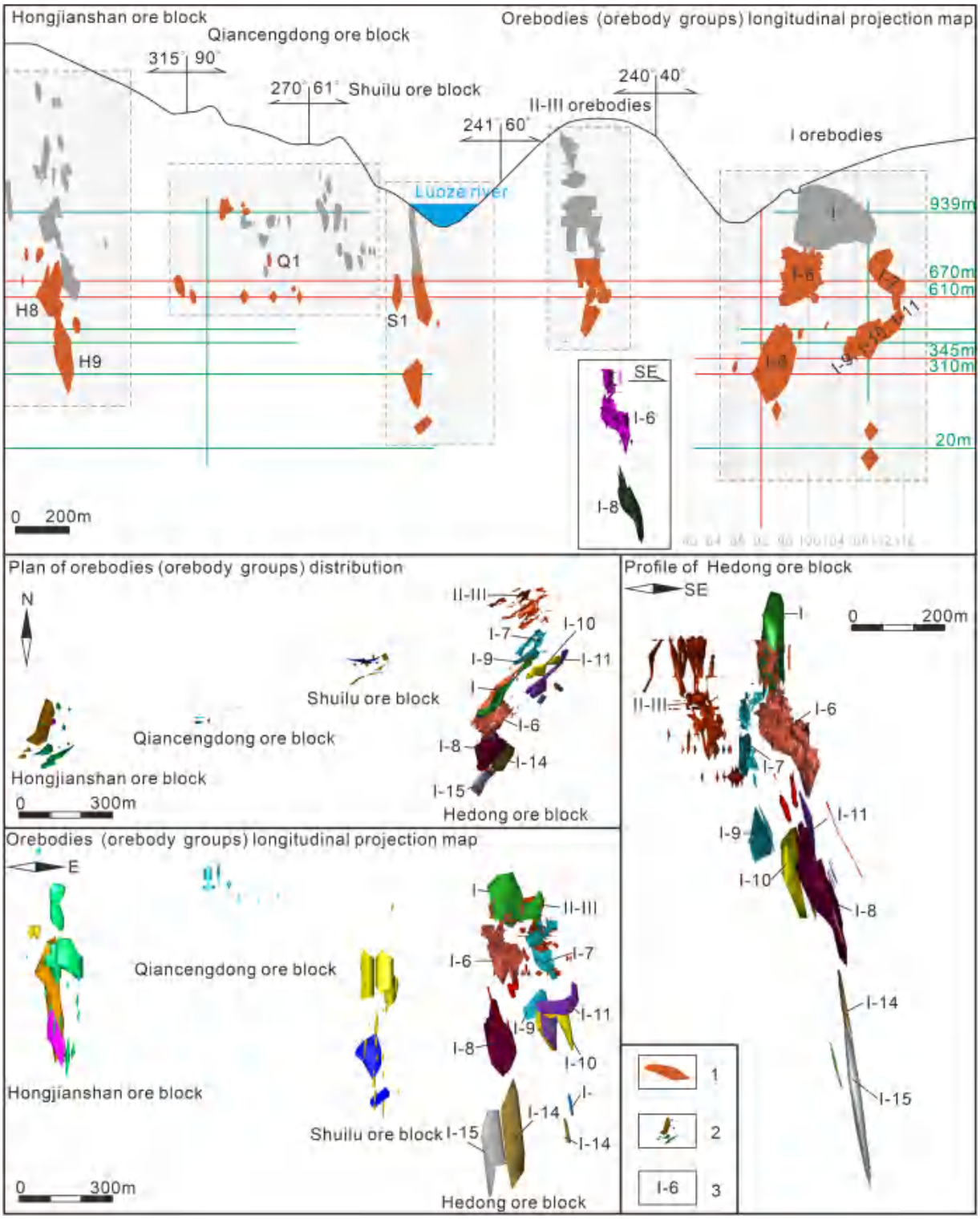

Fig. 2 Plan view and vertical projection of the Maoping germanium-rich lead–zinc deposit ore body distribution (after Wu et al. 2024a). In the vertical projection map, the gray areas represent the mined ore bodies. 1. Known ore bodies; 2. Three-dimensional display; 3. Known ore body numbers

Formation, with NE–SW and NW–SE strikes and dip angles ranging from 70° to 85° (after Han et al. 2024).

3 Sampling and methods

3.1 Sampling

Previous studies have shown that the analysis and testing of tectono-geochemical samples must meet statistical requirements (Zhang et al. 2005). In practical mining situations, difficulties in sample collection within tunnels, insufficient coverage, and other factors often result in sample numbers that do not meet the basic requirements for tectono-geochemical analysis. Therefore, by combining and comprehensively analyzing samples from different sections of tunnels and boreholes, the basic sample quantity requirements can be met.

Therefore, taking the Maoping mining area's surface and deep sections (670 m, 610 m, and 310 m levels and borehole SBDZK670-92–01) as the study objects, tectono-geochemical research is conducted on structural rocks, ore bodies, and mineralized altered rocks (Fig. 3).

4 Research methods

Cluster analysis and factor analysis are effective tools for processing multidimensional data and are capable of extracting the main features of complex variables in

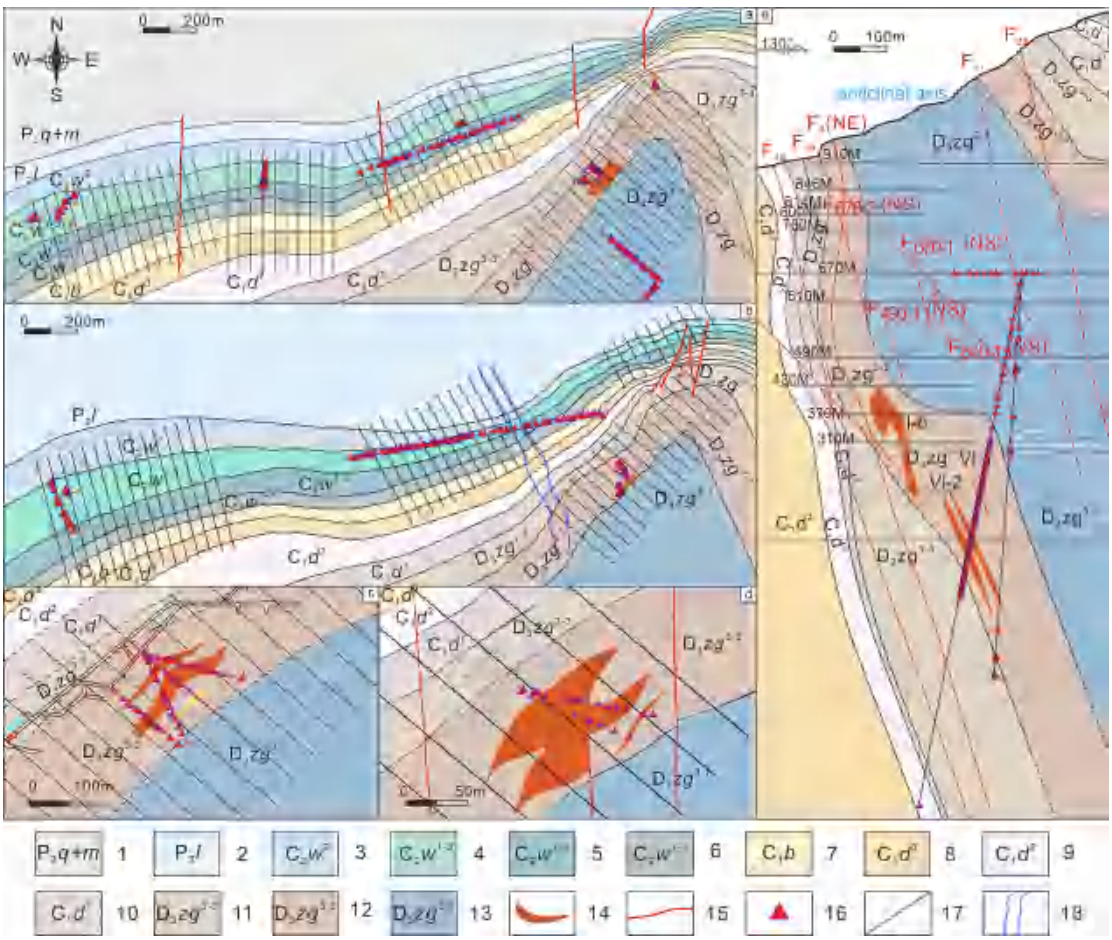

Fig. 3 Sampling location map for the 670 m level (**a**), sampling location map for the 610 m level (**b**), sampling location map for the 310 m level (**c**), sampling location map for the 345 m stratified sampling (**d**), and sampling location map for the 92-line profile (**e**). 1. Middle Permian Qixia + Maokou Formations; 2. Lower Permian Liangshan Formation; 3. Upper Carboniferous Weining Formation; 4. Upper Carboniferous Weining Formation, First Member, Third Submember; 5. Upper Carboniferous Weining Formation, First Member, Second Submember; 6. Upper Carboniferous Weining Formation, First Member, First Submember; 7. Lower Carboniferous Baizuo Formation; 8. Lower Carboniferous Datang Formation, Third Member; 9. Lower Carboniferous Datang Formation, Second Member; 10. Lower Carboniferous Datang Formation, First Member; 11. Upper Devonian Zaige Formation, Third Member, Third Submember; 12. Upper Devonian Zaige Formation, Third Member, Second Submember; 13. Upper Devonian Zaige Formation, Third Member, First Submember; 14. Ore body groups; 15. Faults; 16. Sampling points; 17. Exploration line; 18. Luoze River

geochemical exploration. Factor analysis reduces the data dimensionality and extracts the main geological processes affecting element distribution. Cluster analysis groups elements with similar properties, identifying different types of geochemical anomalies (Men 1979). In complex geological environments, these two methods can reveal the common geological origins of elements, distinguish between background values and anomalies, and thus extract geochemical information related to mineralization. In terms of application, these methods can identify anomalous zones and predict the locations of concealed ore bodies. Factor analysis generates new composite indicators to identify the main anomalous factors, whereas cluster analysis reveals the spatial distribution characteristics of element assemblages, distinguishing mineralization stages and spatial anomaly patterns. This multielement combination approach systematically integrates geological information, efficiently locates geochemical anomaly areas, and improves the accuracy and efficiency of exploration. Therefore, the anomalous zones of mineralization factor scores can be used to infer the enrichment centers of mineralization. High-value zones of different types of mineralization factor scores can be used to analyze the mineralization types of concealed ore bodies. The anomalous zonation characteristics of different mineralization element assemblages can be used to infer the direction of mineralizing fluids and analyze the head and tail halos of concealed ore bodies. Additionally, geochemical anomalies that characterize hydrothermal alteration can be used to elucidate the relationship between hydrothermal alteration and mineralization enrichment, thereby inferring favorable ore-forming locations and achieving the goal of predicting concealed ore bodies (Han 2005; Han et al. 2015; Zhao et al. 2015; Qiu et al. 2017).

The premise of applying mathematical statistical methods to sample analysis is that the elements follow a normal or log-normal distribution. Through R-type factor analysis, the anomalous characteristics of each factor element combination are studied, the lower limit of anomalies is determined, and the anomalous zones are then delineated.

Representative samples were collected from the 670, 610, and 310 m levels, as well as the 92 exploration line profile borehole. A total of 383 samples were collected.

Owing to extensive shotcrete support in underground tunnels, handheld drilling rigs were employed for equidistant intensive sampling. In areas covered by drill holes, horizontal and deep drill cores were logged and sampled. The sampling details are as follows:

670 m Level: Main tunnel: 19 samples from $C_2w^{1\text{-}2}$, 8 samples from $C_2w^{1\text{-}3}$; Hedong ore block: 20 samples from $D_3zg^{3\text{-}1}$, 11 samples from $D_3zg^{3\text{-}2}$, 3 samples from $D_3zg^{3\text{-}3}$; Hexi Shuilu ore block: 5 samples from $C_2w^{1\text{-}3}$; Hexi Qiancengdong ore block: 11 samples from $C_2w^{1\text{-}3}$, 1 sample from $C_2w^{1\text{-}2}$; Hexi Hongjianshan ore block: 12 samples from $C_2w^{1\text{-}3}$.

610 m Level: Main tunnel: 2 samples from C_1d^3, 4 samples from C_1b, 5 samples from $C_2w^{1\text{-}1}$, 4 samples from $C_2w^{1\text{-}2}$, 41 samples from $C_2w^{1\text{-}3}$, 2 samples from C_2w^2; Hedong ore block: 10 samples from $D_3zg^{3\text{-}2}$; Hexi Hongjianshan ore block: 25 samples from $C_2w^{1\text{-}3}$, 1 sample from $C_2w^{1\text{-}2}$; 310 m Level: 51 samples from $D_3zg^{3\text{-}2}$; 345 m sublevel: 23 samples from $D_3zg^{3\text{-}2}$

Line 92 profile deep drilling: 125 samples (30 from D_3zg^{3-1}, 75 from D_3zg^{3-2}, 19 from D_3zg^{3-3}, and 1 from C_1d^2).

In total, the deep mining area yielded 121 samples from C_2w; 5 samples from C_1b; 3 samples from C_1d; and 242 samples from D_3zg.

A total of 19 elements closely related to the normal distribution model and metallogenic process were analyzed: Sn, As, Sb, Hg, Ga, Rb, Sr, Ni, Mn, Mo, Cu, Zn, Ba, Co, Cr, Cd, Pb, Tl, Ge, and In. Element analysis was completed at the Northwest Geological and Mineral Resources Testing Center of the Xi'an Institute of Nonferrous Metals. Through cluster and factor analysis of the elemental content data from structural rocks within faults, the distribution patterns of anomalies in major ore-forming elements, ore-related indicator elements, and ore-related element combinations were clarified. Information on low–weak mineralization in the deep parts of the deposit was extracted, and exploration target areas were delineated.

5 Results

5.1 R-type cluster analysis

By performing R-type cluster analysis on the elemental data from structural rock samples in the tunnel, an element composition dendrogram was obtained. When the distance coefficient D = 12, the 19 elements were grouped into four clusters (Fig. 4):

Group I: Zn, Pb, As, Sb, Cd, Hg, Ge, Cu, and In;
Group II: Rb, Tl, and Mo;
Group III: Ba and Ga;
Group IV: Co, Ni, and Cr.

5.2 R-type factor analysis

R-type factor analysis was conducted on 383 structural rock samples closely related to mineralization and 19 elements. The data were tested via the Kaiser–Meyer–Olkin (KMO) test, where a KMO value closer to 1 indicates stronger data correlation. The test results show a KMO

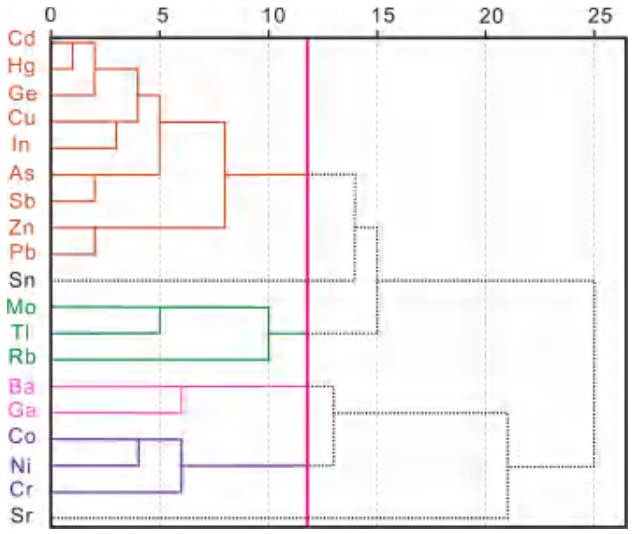

Fig. 4 R-type cluster analysis dendrogram of tectonic rocks in the Maoping Pb–Zn deposit

Table 1 Varimax rotated factor loading matrix for factor analysis of structural rocks in the Maoping Pb–Zn mine tunnel

Element/Factor	F1	F2	F3	F4	F5
Cd	0.93	−0.184	0.016	0.032	−0.003
Cu	0.908	0.224	0.056	−0.037	0.08
Ge	0.88	0.004	0.282	0.125	0.086
Zn	0.862	−0.236	0.166	0.013	0.068
Sb	0.858	−0.056	0.363	−0.095	−0.052
In	0.857	0.168	0.121	−0.095	0.071
Pb	0.823	−0.191	0.262	−0.016	0.111
Sr	−0.719	0.18	−0.199	0.189	−0.106
As	0.698	−0.091	0.592	−0.036	−0.021
Hg	0.649	−0.208	0.387	0.023	−0.465
Ni	−0.246	0.876	0.096	0.047	−0.003
Co	−0.202	0.861	0.004	0.168	0.153
Cr	0.109	0.85	0.107	0.234	0.183
Rb	−0.041	0.647	0.561	0.279	0.053
Tl	0.459	0.186	0.814	0.043	0.072
Mo	0.318	0.182	0.802	−0.137	0.006
Ba	−0.227	0.234	−0.068	0.895	0.109
Ga	0.182	0.557	0.034	0.738	0.011
Sn	0.38	0.358	0.129	0.17	0.764

value of 0.876, which exceeds the threshold of KMO > 0.6 as defined by Kaiser (Kaiser 1974). Additionally, the significance probability (Sig) value of Bartlett's sphericity test is less than the 0.05 significance level. These results indicate that there is sufficient correlation within the data, making it suitable for R-type factor analysis. When the cumulative variance contribution reaches 84.4%, five factors can be extracted (Table 1).

F1: Cd, Cu, Ge, Zn, Sb, In, Pb, Sr(-), As, Hg;
F2: Ni, Co, Cr, Rb, Ga;
F3: Rb, Mo, Tl, As;
F4: Ba, Ga;
F5: Sn

The F1 factor (Cd-Cu-Ge-Zn-Sb-In-Pb-Sr(-)-As-Hg) represents medium- to low-temperature ore-forming elements (an element assemblage that overlaps with mineralization halos and proximal halos); the F2 factor (Ni-Co-Cr-Rb-Ga) represents a tail halo element assemblage associated with mineralization; the F3 factor (Rb-Mo-Tl-As) represents a front halo element assemblage associated with mineralization; the F4 factor (Ba-Ga) represents an element assemblage related to baritization; and the F5 factor (Sn) has unclear significance.

5.3 Geochemical anomaly delineation

On the basis of the results of cluster analysis and factor analysis, structural geochemical anomaly–geological maps at different levels were generated using SURFER 15 and MapGIS 6.7 (Figs. 5, 6, 7, 8, 9). The structural geochemical anomalies at different levels exhibit similar characteristics, with distributions concentrated near the ore bodies. A comprehensive analysis of the anomalous distribution characteristics of various element assemblages was used to delineate anomaly zones (Fig. 5). The primary anomaly zones are located near the ore bodies, with the anomaly zones of different element assemblages distributed at various positions around the ore bodies. Furthermore, the anomaly gradient decreases progressively from the ore body center to its periphery.

6 Discussion

6.1 Indicative significance of deep low–weak mineralization information

Through the geochemical characteristics analysis of borehole SBZK-670–92-01 (Fig. 6), the element combinations of different factors show strong correlations. Among them, the high values of the F1 factor's element combination are concentrated within the ore body and gradually decrease toward both sides. The element combination of the F2 factor shows high values in the deep parts of both sections of the ore body but lower contents within the ore body itself. The element combination of the F3 factor results in high values at the top of the ore body and within the ore body, with its content gradually decreasing toward the deeper parts.

The element combination information from borehole SBZK-670–92-01 (Fig. 7) shows that the anomalies of the

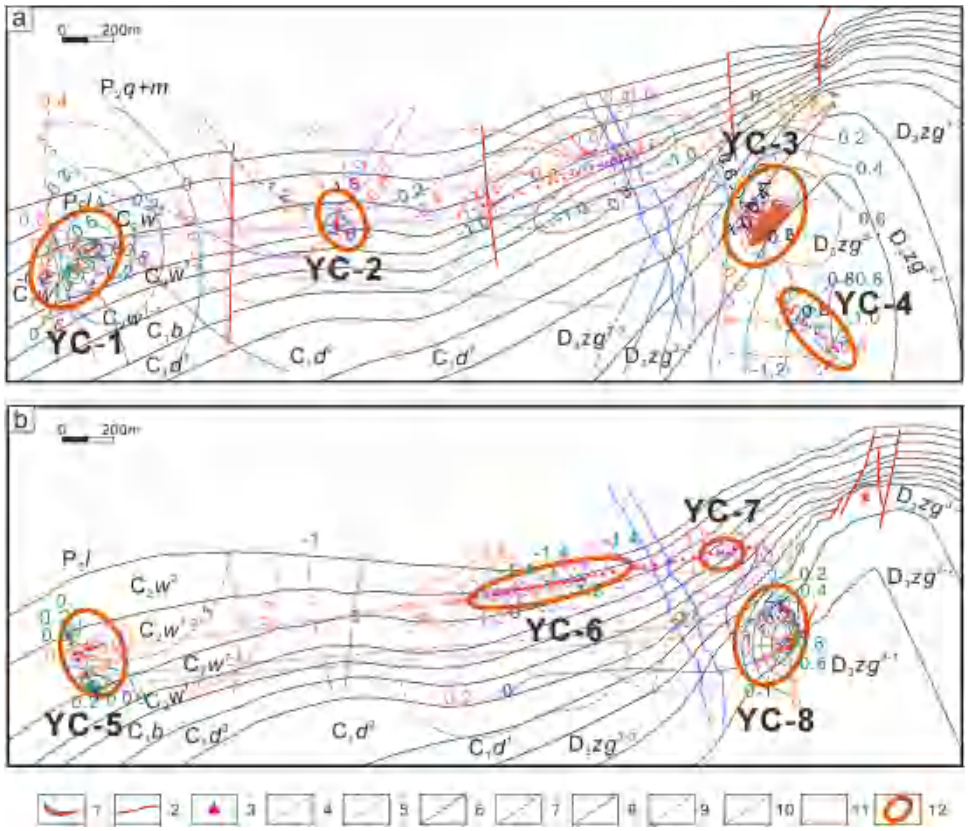

Fig. 5 Geochemical anomaly geological map of the 670 m level (**a**), geochemical anomaly geological map of the 610 m level (**b**). 1. Ore body groups; 2. Faults; 3. Sampling points; 4. Positive anomalies in the F1 factor element assemblage; 5. Negative anomaly of the F1 factor element assemblage; 6. Positive anomalies in the F2 factor element assemblage; 7. Negative anomaly of the F2 factor element assemblage; 8. Positive anomaly of the F3 factor element assemblage; 9. Negative anomaly of the F3 factor element assemblage; 10. Positive anomaly of the F4 factor element assemblage; 11. Negative anomaly of the F4 factor element assemblage; 12. Geochemical anomaly area

mineralization factor F1 element combination overlap or are adjacent to the anomalies of the individual elements Pb and Zn. The anomalous combinations of different factor element combinations reflect information about deep ore bodies, serving as an important basis for delineating key exploration target areas. The high anomaly zone of the F1 factor almost overlaps with the known ore body, representing a mineralization halo. The high anomaly of the F2 factor appears in the deep part of the ore body, representing a tail halo. The element combination anomalies of the F3 and F4 factors show high anomaly values in the shallow part of the ore body, representing front halos. Therefore, the anomalous element combinations of the F1, F2, F3, and F4 factors can indicate deep mineralization information.

To clarify the spatial distribution characteristics of geochemical anomalies near the ore body, structural geochemical anomaly maps were integrated with geological features. The results indicate the following.

The high anomaly zones of the F1 factor element combination closely coincide with the ore body, and the distribution of the front halo and tail halo aligns with the plunge direction of the known ore body (Figs. 2, 8, and 9). This finding provides clear indications of the spatial distribution of the ore body. Additionally, near the H8 ore body in the Hexi area and the I-6 ore body in the Hedong area (Fig. 8), the anomalous distributions of the tail halo and front halo exhibit significant directional differences, indicating that the ore bodies in different mining sections have distinct lateral trends and extension characteristics.

The vertical analysis (Fig. 9) reveals that from 345 to 310 m, the anomaly values of the F1 and F2 factor element combinations decrease, whereas the Zn anomaly values increase with depth, and the Pb anomaly values decrease. This variation reflects a Pb-high and Zn-low characteristic at the ore body center and a Zn-high and Pb-low characteristic at the ore body periphery. Additionally, the F4 factor (front halo) tends to increase with increasing depth, suggesting the potential presence of larger concealed ore bodies at greater depths. This provides a prospective target for further deep exploration.

Geochemical anomaly comparisons at different depths (Fig. 8) reveal that the high anomaly zones of the F1 and F2 factors are significantly larger at the 670 m level than at the 610 m level, whereas the F4 factor anomaly is more prominent at the 610 m level. These spatial distribution differences are closely related to ore-controlling factors such as structure, wall rock alteration, and mineralization temperature. In particular, the negative correlation between the tail halo element combination (F2) and the front halo element combinations (F3 and F4) further highlights the indicative role of different element combinations in the ore body distribution.

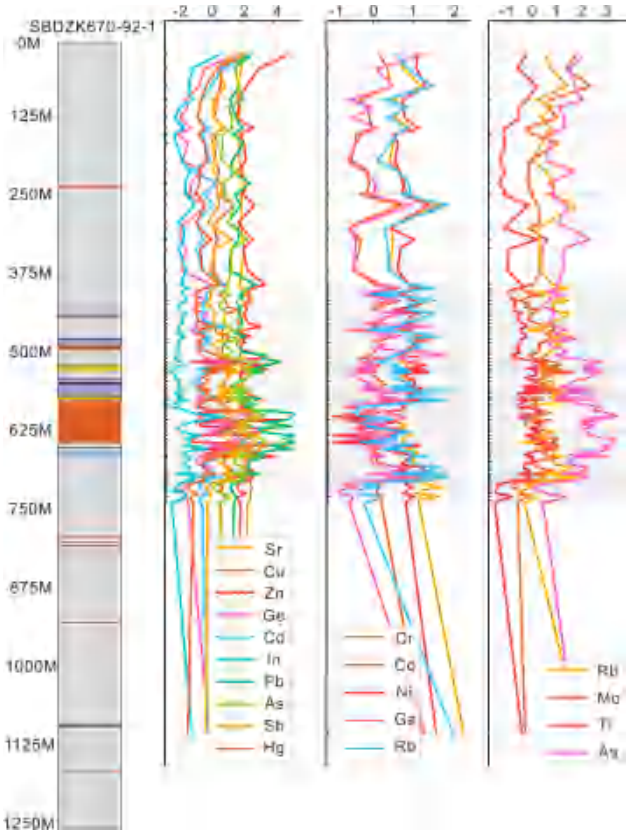

Fig. 6 Element anomaly variation chart of borehole SBDZK670-92–1

6.2 The enhancement effect of element combination anomalies

A comparison of the single-element anomaly distribution maps with the element combination anomaly distribution maps reveals that the distribution characteristics of the element combination anomalies are more pronounced. Taking Pb and Zn as examples (Fig. 10), the anomalies of the two elements individually are mainly concentrated in the distribution areas of known ore bodies, with almost no anomalies in other sections. In the SBDZK670-92–1 borehole data, element combination anomalies are not only evident in the shallow and deep parts of the known ore body but also exhibit distinct distribution characteristics in the surrounding areas of the ore body (Fig. 7). This anomalous distribution supports the geochemical characteristic analysis of the front halo, mineralization halo, and tail halo of the ore body, providing an effective basis for the extraction of mineralization information. Moreover, a comparison of multielement combination anomaly variation maps with Pb and Zn single-element contents reveals that the high anomaly zones of single elements are confined to areas near the ore body, whereas anomalous signals in other sections are relatively weak or even absent. In contrast, element combination anomalies can effectively amplify mineralization signals, allowing even low-intensity mineralization information to be clearly displayed and forming more coherent anomalous zones. This

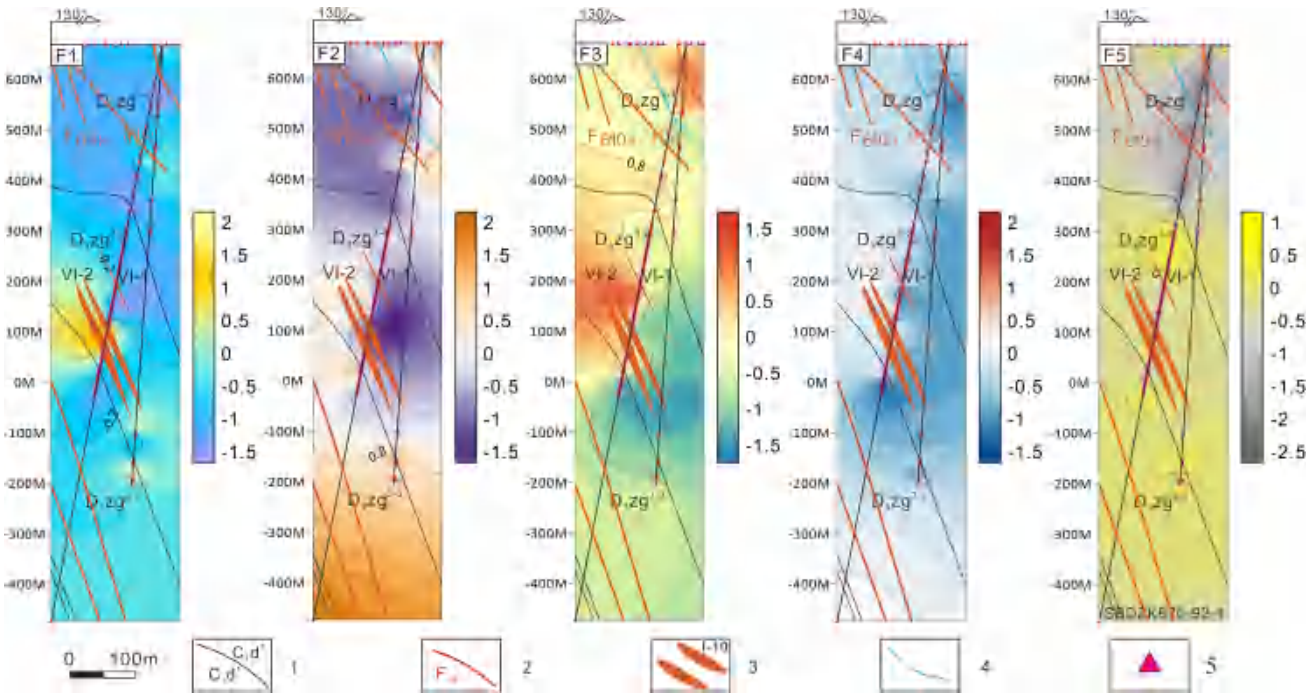

Fig. 7 Element combination anomaly profile of the 92 exploration line cross-section. 1. Stratigraphic boundary; 2. Faults and fault numbers; 3. Known ore body numbers; 4. Anticline axis; 5. Sampling points

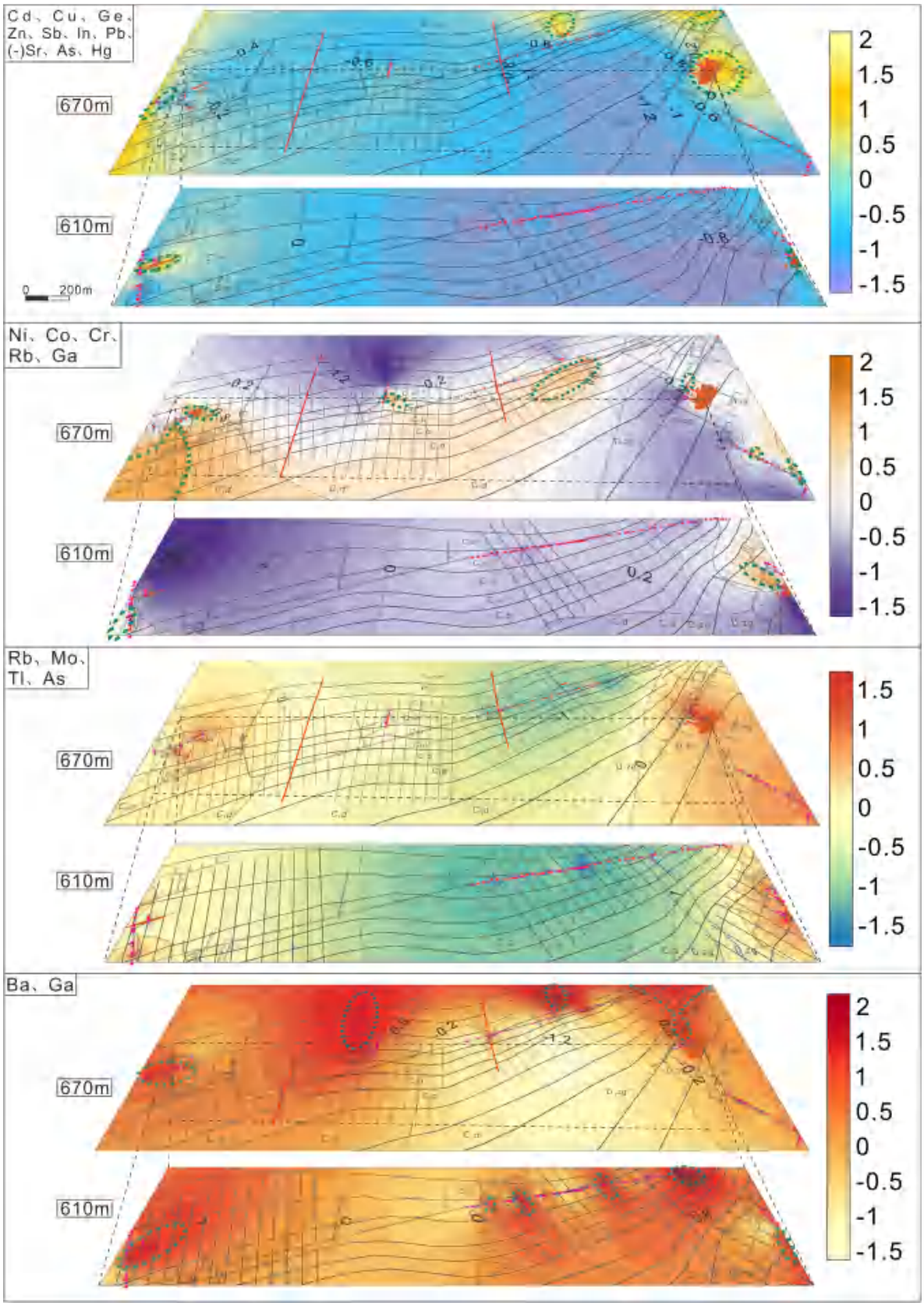

Fig. 8 Structural geochemical anomalies at 670 m and 610 m

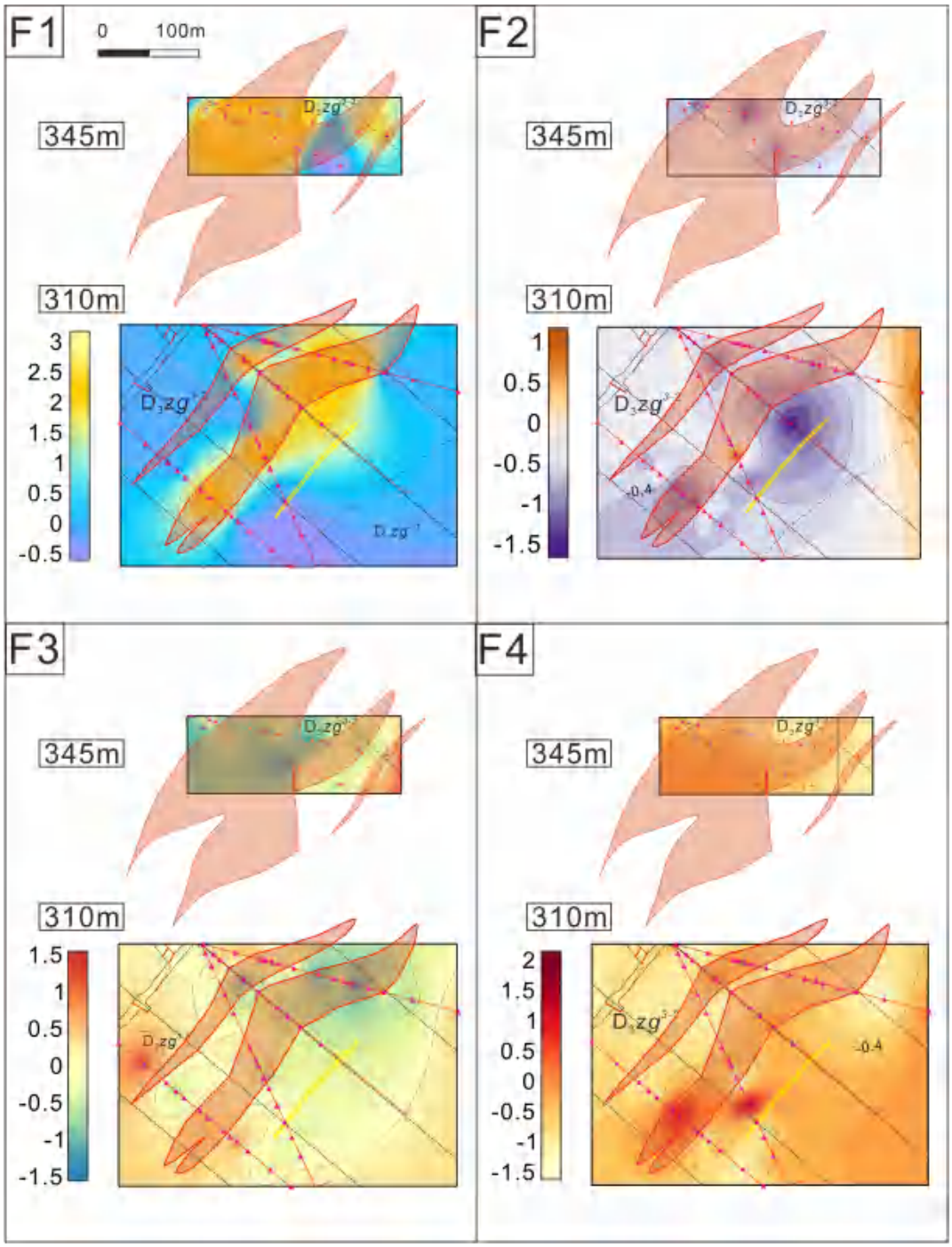

Fig. 9 Structural geochemical anomalies at depths of 345 m and 310 m

characteristic is particularly advantageous under complex geological conditions, assisting in the extraction of deep mineralization information.

In summary, the multielement combination method enables comprehensive consideration of mineralization characteristics at different depths and ore-controlling structures, thereby fully revealing the formation and distribution patterns of ore bodies. This approach is not only applicable to the analysis of known ore bodies but also effectively identifies geochemical anomalies over broader areas.

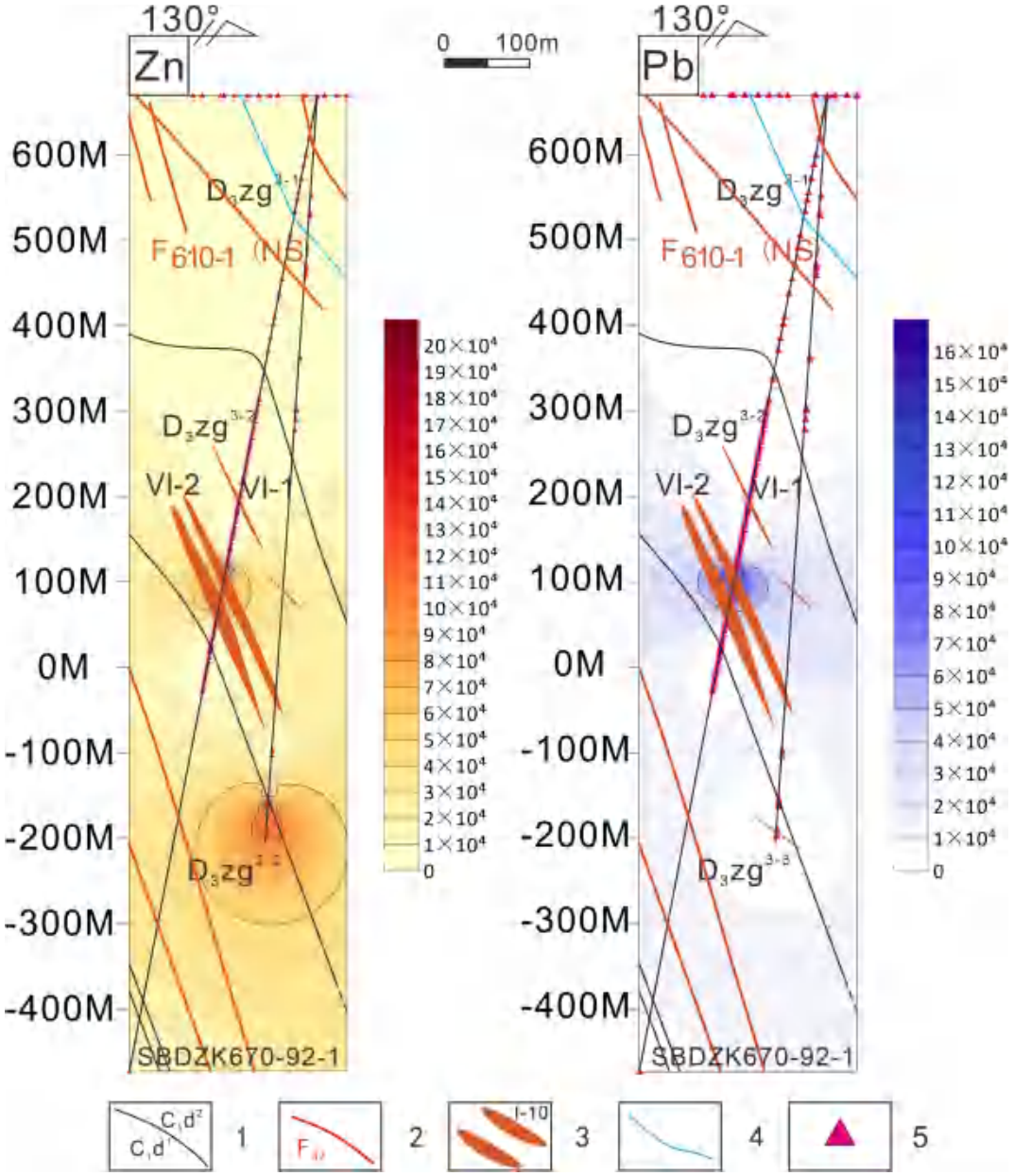

Fig. 10 Zn and Pb element anomalies in the 92 exploration line: 1. Stratigraphic boundary; 2. Fault and fault number; 3. Known ore body number; 4. Anticline axis; 5. Sampling point

6.3 Spatial variation characteristics of element combination geochemical anomalies

6.3.1 Linear variation in anomalies

The element combination anomalies of Pb, Zn, and the F1 factor exhibit strong correlations in the deep drilling profile SBDZK670-92–1 of the 92 exploration line (Fig. 11). The Pb, Zn, and F1 factor element combination anomalies are greater within the ore body, whereas their contents in the adjacent wall rocks show a significant decreasing trend. Although the overall Pb and Zn contents in the deep wall rocks are lower than those in the ore body, the Pb and Zn contents in the wall rocks near the ore body are higher than those in more distant wall rocks. These findings indicate that Pb–Zn mineralization caused the mineralizing fluids to be "injected" into favorable structural positions within the wall rocks. In addition, the contents of Pb and Zn in the surrounding rock near the roof are slightly higher than those in the surrounding rock near the floor.

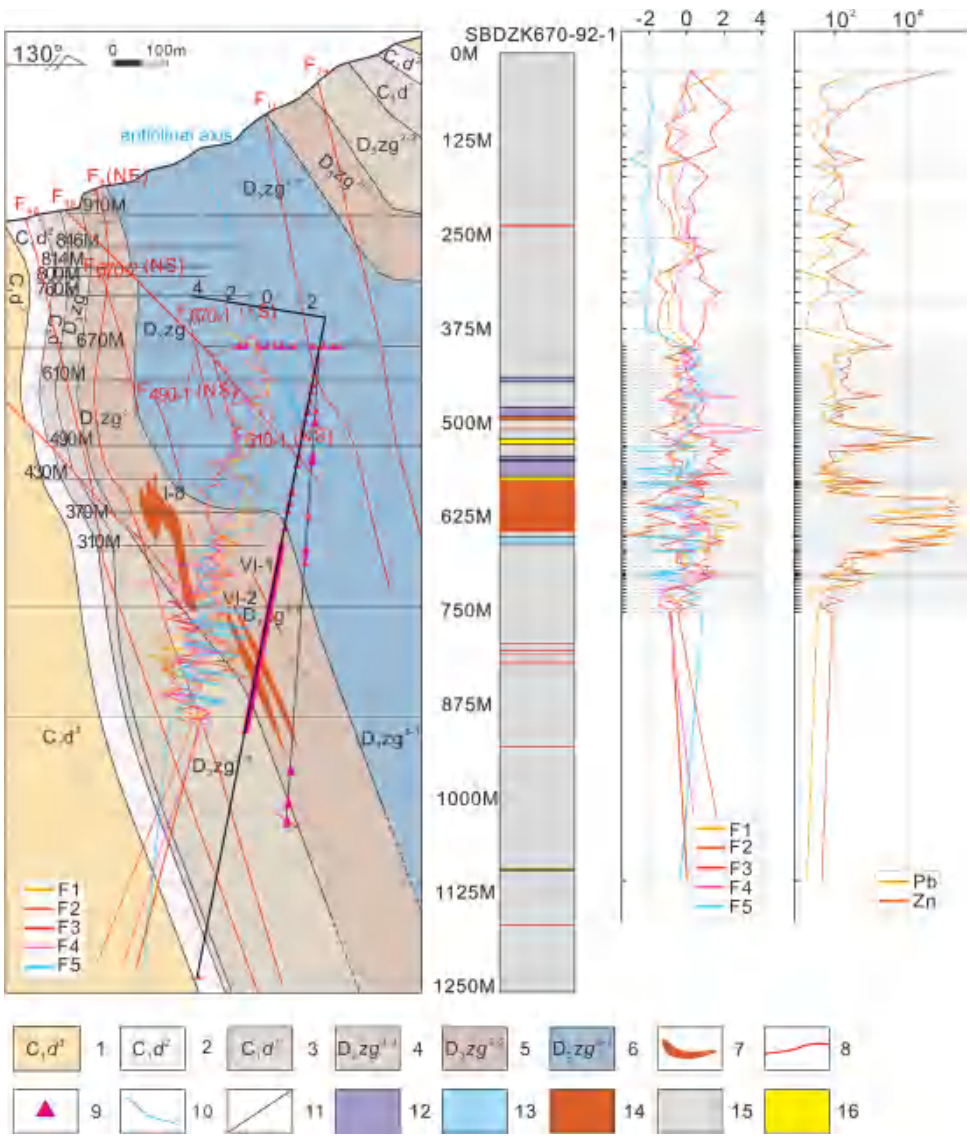

Fig. 11 Element and factor combination anomaly profile of deep borehole SBDZK670-92–1. 1. Lower Carboniferous Datang Formation, Third Member; 2. Lower Carboniferous Datang Formation, Second Member; 3. Lower Carboniferous Datang Formation, First Member; 4. Upper Devonian Zaige Formation, Third Member, Third Submember; 5. Upper Devonian Zaige Formation, Third Member, Second Submember; 6. Upper Devonian Zaige Formation, Third Member, First Submember; 7. Ore body groups; 8. Faults; 9. Sampling points; 10. Anticline axis; 11. Level; 12. Dolomitization; 13. Calcification; 14. Lead–zinc ore body; 15. Wall rock; 16. Pyritization

6.3.2 Planar anomaly variation

The Zn anomalies in the Hedong mining section are primarily concentrated near the I-6 ore body, whereas the Pb anomalies are significantly concentrated near the Hongjianshan H8 ore body in the Hexi mining section (Fig. 12). This phenomenon indicates differences in the main elemental compositions of the Hedong and Hexi ore bodies, possibly reflecting the influence of different geological processes during mineralization.

The anomalies of the F1 factor element combination in the Hedong mining section are distributed mainly between Line 96 and Line 106 near the I-6 ore body and the sulfide ore locations on the northern part of Line 116 to Line 118. Additionally, the Shuilu and Hongjianshan mining sections also present relatively high anomaly values. The anomalies of the F2 factor element combination at the 670 m level are predominantly distributed on the southern side, with the maximum anomalies observed on the southwestern side of the Hongjianshan mining section and the southern side of the main transportation tunnel in the Hexi area. Anomalously high values are also found near the Line 92 cross-vein and the I-6 ore body in the Hedong area, whereas the northern part of the Qiancedong mining section presents relatively high negative anomalies. The anomalies of the F4 factor element combination are primarily distributed on the northern side, with higher anomaly values in the Shuilu and Qiancedong mining sections. Elevated anomalies are also observed in the Hongjianshan mining section, the I-6 ore body, and the sulfide ore locations on the northeastern side between Line 116 and Line 118 (Fig. 13).

On the basis of the deep anomaly distribution of the F2 factor element combination, it is generally located in the NW direction of the F1 factor element combination

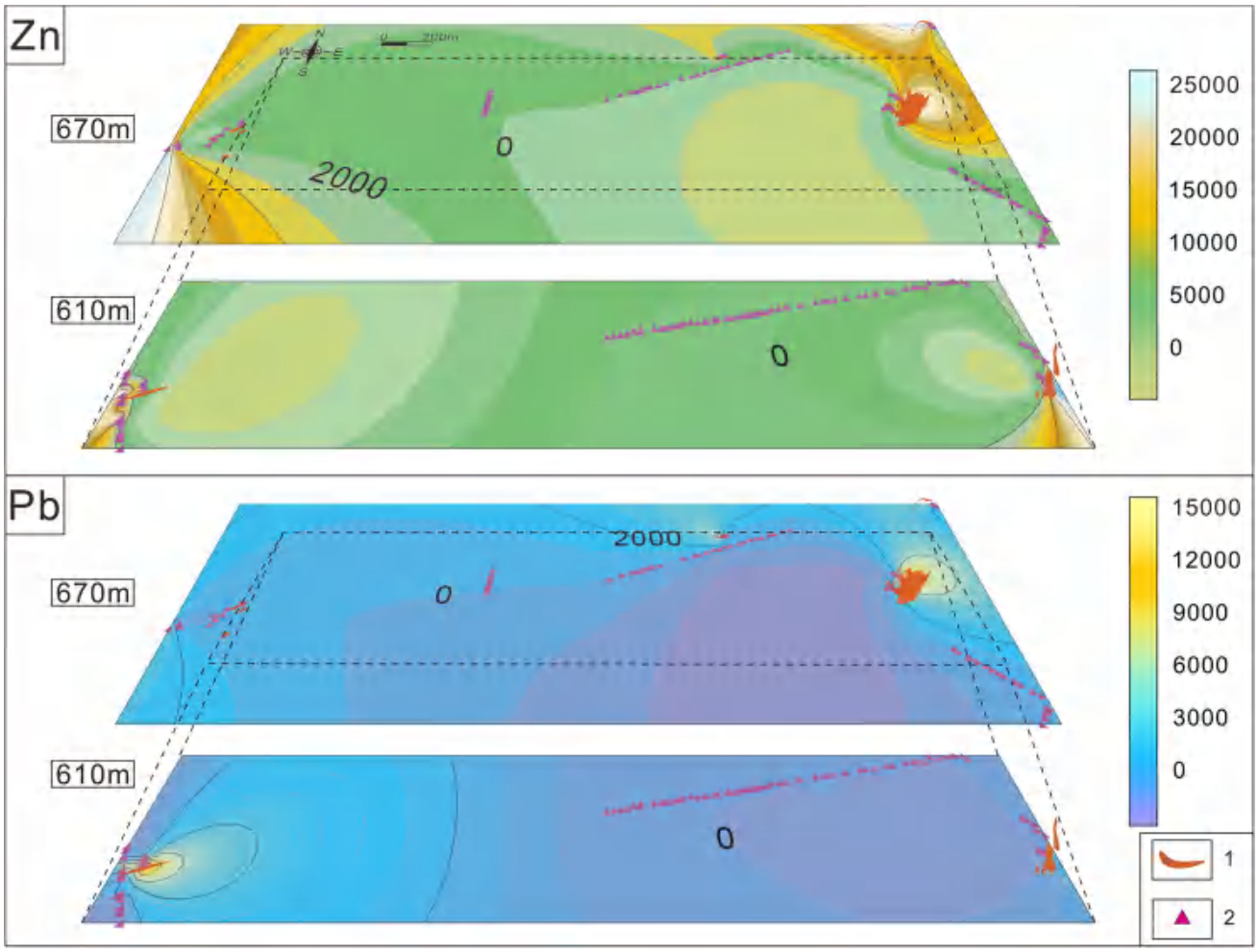

Fig. 12 Planar anomaly maps of Pb and Zn contents at 670 m and 610 m. 1. Ore body; 2. Sampling point

anomaly zone and extends deeper. The anomaly zone of the F3 factor element combination, on the other hand, is situated in the SE direction of the F1 anomaly and is distributed in shallow areas or partially overlaps with the F1 factor anomaly zone. Additionally, the anomaly zone of the F2 factor element combination remains open in the deep NW direction. The anomaly zones of the F1, F2, and F3 factor element combinations exhibit adjacent or partially overlapping characteristics.

From the perspective of single-element anomalies, the overall anomaly values of Zn are greater than those of Pb, with a larger anomalous range in the Hedong area than in the Hexi area. The anomaly values in the deeper parts are significantly greater than those in the shallow parts, indicating that the intensity of hydrothermal alteration in the deeper parts is more pronounced than that in the shallow parts. Therefore, the concealed mineralization zones and ore bodies of this deposit may extend deeper, indicating further exploration potential.

This study revealed that the spatial distribution of mineralization elements in the ore body exhibits certain gradient characteristics. By analyzing the gradient variation features of geochemical anomalies, the lateral trend direction of the ore body can be indirectly inferred.

The distribution characteristics of geochemical anomalies are constrained by the dip direction of the ore body. The mineralization process often extends along the dip direction of the ore body, resulting in a spatial gradient distribution of element concentrations around the ore body. The extension direction of structural geochemical anomalies indicates the strike of concealed ore (mineralized) bodies, whereas the gradient of structural geochemical anomalies can suggest the dip direction of concealed ore bodies. Additionally, the "drift" direction of structural geochemical mineralization anomalies at different depths can indicate the lateral trend direction of the ore (mineralized) body (Han 2005). Therefore, structural analysis of geochemical anomalies can reveal the dip characteristics

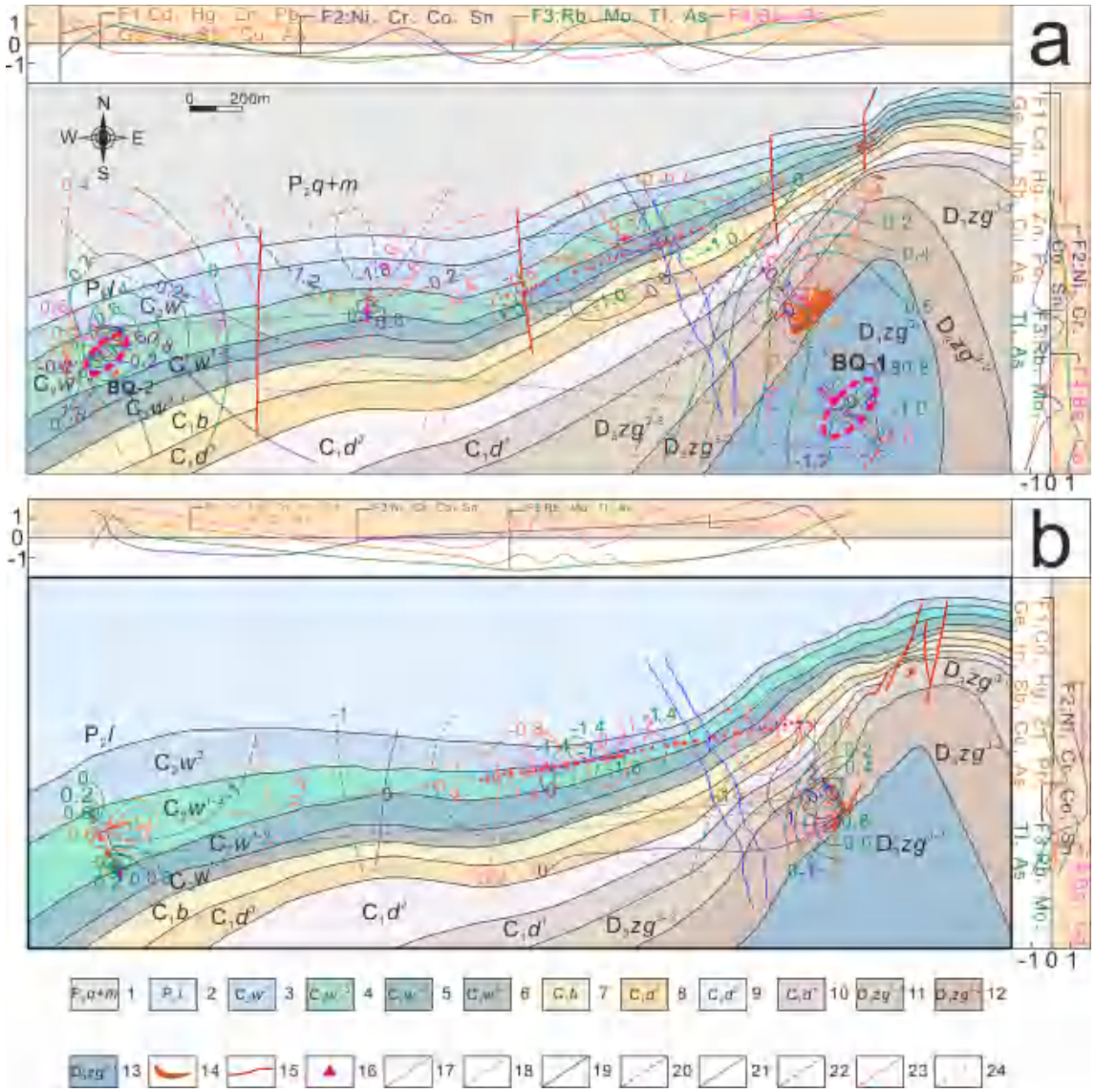

Fig. 13 Target area prediction map for the 670 m level (**a**). Target area prediction map for the 610 m level (**b**). 1. Middle Permian Qixia + Maokou Formations; 2. Lower Permian Liangshan Formation; 3. Upper Carboniferous Weining Formation; 4. Upper Carboniferous Weining Formation, First Member, Third Submember; 5. Upper Carboniferous Weining Formation, First Member, Second Submember; 6. Upper Carboniferous Weining Formation, First Member, First Submember; 7. Lower Carboniferous Baizuo Formation; 8. Lower Carboniferous Datang Formation, Third Member; 9. Lower Carboniferous Datang Formation, Second Member; 10. Lower Carboniferous Datang Formation, First Member; 11. Upper Devonian Zaige Formation, Third Member, Third Submember; 12. Upper Devonian Zaige Formation, Third Member, Second Submember; 13. Upper Devonian Zaige Formation, Third Member, First Submember; 14. Ore body groups; 15. Faults; 16. Sampling points; 17. Positive anomaly of the F1 factor element assemblage; 18. Negative anomaly of the F1 factor element assemblage; 19. Positive anomaly of the F2 factor element assemblage; 20. Negative anomaly of the F2 factor element assemblage; 21. Positive anomaly of the F3 factor element assemblage; 22. Negative anomaly of the F3 factor element assemblage; 23. Positive anomaly of the F4 factor element assemblage; 24. Negative anomaly of the F4 factor element assemblage

of concealed ore bodies. The distribution of the F1 factor element combination anomalies aligns well with the currently identified NNE–SSW-trending ore body (Figs. 8 and 9). The F3 and F4 element combination anomalies in the deeper sections generally exhibit relatively high values and are distributed on the SW side of the ore body (Fig. 9). These findings indicate that the Hedong ore body generally trends laterally toward the SW, which is consistent with the currently identified ore body.

6.4 Migration pattern of the ore-forming fluid

The regular arrangement of different types of mineralization factor combination anomalies on various planes (resulting

from the sequential appearance of different mineralization elements as the temperature of the hydrothermal fluids decreases) can reflect the flow direction of the fluids (Wang et al. 2016). Studies have shown that the migration directions of ore-forming fluids in the Hedong and Hexi mining sections were not consistent (Fig. 14).

In the Hedong mining section, at the 610 and 670 m levels, horizontal zonation of the F1 (mineralization halo), F2 (tail halo), and F3 (front halo) factor element combinations is observed from the ore body center to the SE and NW sides, respectively. This pattern reflects the migration of ore-forming fluids from the SE at depth to the NW at shallower levels. Specifically, the tail halo is greater on the SE side of the ore body and decreases toward the NW side, whereas the front halo is greater on the NW side and decreases toward the SE side.

In the Hexi mining section, at the 610 and 670 m levels, horizontal zonation of the F1 (mineralization halo), F2 (tail halo), and F3 (front halo) factor element combinations is observed from the ore body center to the SW and NE sides, respectively. This pattern reflects the migration of ore-forming fluids from the SW at depth toward the NE at shallower levels. Specifically, the tail halo is greater on the SW side of the ore body and decreases toward the NE side, whereas the front halo is greater on the NE side and decreases toward the SW side.

Therefore, it is reasonable to infer that during the mineralization period, fluids migrated from deep to shallow levels along the ore-guiding structure (Maoping Fault) in two main directions. In one case, fluids migrated from the deep SE to the shallow NW, first entering the ore-controlling structures and preferentially reaching the D_3zg ore-hosting formation. The fluids then further migrated into the C_2w ore-bearing strata. Within the extensional spaces of NE–SW-trending left-lateral compressive-shear interlayer faults in the ore-hosting formations (specifically, the "gentle–wide, steep–narrow" spaces), the fluids underwent decompression, forming the lead–zinc ore bodies in the Hedong mining section. In the other case, fluids migrated from the SW at depth to the NE at shallower levels. After entering the ore-controlling structures, they reached the C_2w ore-hosting formation. Similarly, the fluids experienced decompression in the extensional spaces of NE–SW-trending left-lateral compressive-shear interlayer faults, resulting in the formation of the lead–zinc ore bodies in the Hexi mining section. Therefore, it is inferred that the mineralizing fluids also passed through and precipitated within the D_3zg formation in the deeper parts of the Hexi mining section. This suggests

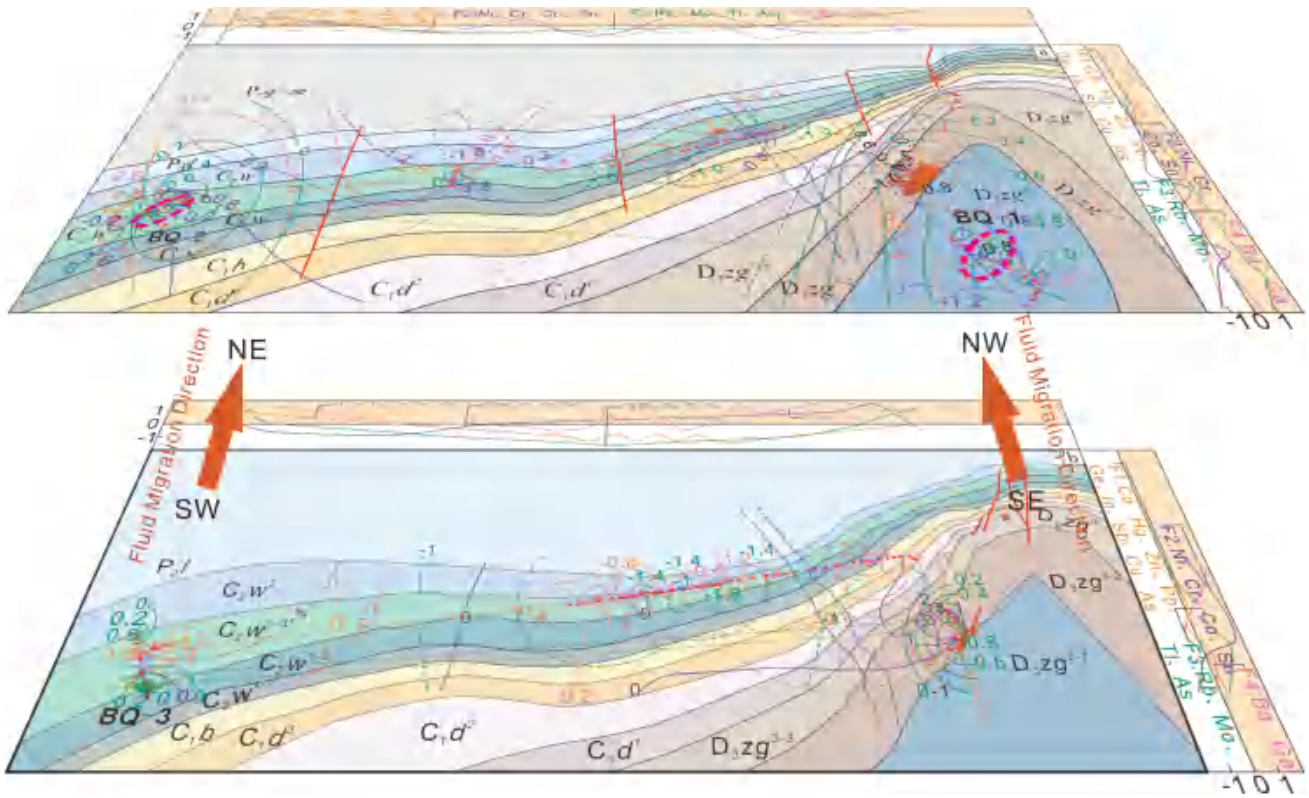

Fig. 14 Schematic diagram of the fluid migration direction

the possible presence of concealed ore bodies in the D3zg formation at deeper levels of the Hexi mining section.

6.5 Geochemical deep anomaly evaluation criteria

On the basis of the geological characteristics of the deposit, the tectono-geochemical anomaly indicators are as follows:

6.5.1 Comprehensive element anomaly indicators

The intensity and scale of the vertical mineralization halos are weaker in the shallow parts and stronger in the deeper parts. A comprehensive study of the spatial variation in element combination geochemical anomalies suggests that the concealed mineralized zone may continue to extend deeper, indicating favorable prospects for deep ore exploration.

On the basis of the vertical variation in the element combination of tectono-geochemical anomalies, both the front halo and the mineralization halo in the deeper parts of the known ore body show increasing trends. This suggests that there may be more concealed ore bodies in the deeper parts of the I ore body group and VI ore body group in the Hedong area (Fig. 9). Additionally, the vertical variation pattern of the mineralization halo is consistent with the actual lateral trend pattern of the ore bodies within the deposit. At greater depths, the scale of the ore body and the extent of surrounding mineralization are inferred to gradually increase. Therefore, element combination geochemical anomaly information can serve as an indicator of the extension of concealed ore bodies into deeper regions (Fig. 15).

6.5.2 Lateral trend direction of concealed ore bodies

On the basis of the anomalies of different factor element combinations (the "drift" direction of tectono-geochemical mineralization anomalies can indicate the lateral trend direction of ore bodies), the lateral trend direction of the ore body can be inferred (Han 2005).

In the Hedong mining section, the anomaly gradient of the mineralization factor F1 diverges from SW to NE, reflecting the lateral extension of concealed ore bodies in the NW–SE direction. The high degree of anomaly overlap among multiple factor element combinations (F2, F3, and F4) near the ore body indicates steeply dipping ore-hosting structures (concealed ore bodies). The anomaly gradients of different element combinations weaken progressively from the ore body center to the periphery in the ENE–WSW direction, indicating a decrease in mineralization anomalies in the NEE–SWW direction (Figs. 5, 6, 7, 8, 9).

In the Hexi mining section, the anomaly gradient of the mineralization factor F1 diverges from NE to SW, reflecting the lateral trending extension of concealed ore bodies in the SW–NE direction. The high degree of anomaly overlap among multiple factor element combinations (F2, F3, and F4) near the ore body indicates steeply dipping ore-bearing structures and concealed ore bodies (Fig. 13).

6.5.3 Spatial coupling relationships between anomalies and ore bodies

(1) Planar coincidence: The high-value zones of the F1 factor anomalies (Cd-Cu-Ge-Zn-Sb-In-Pb-Sr(-)-As-Hg) exhibit an extremely high degree of overlap with the planar projections of known ore bodies (Figs. 8, 9), indicating precise delineation of mineralization halos along the ore boundaries.
(2) Vertical anomalies: The F3 (front halo) and F2 (tail halo) factor anomalies display an approximately mirror-like distribution in the vertical direction (Fig. 11). Taking the SBDZK670-92–1 drill hole on Line 92 as an example, the F3 anomaly peak occurs near the roof of the ore body (approximately 0 m), whereas the F2 anomaly peak is concentrated near the floor of the ore body (approximately −200 m), revealing the spatial occurrence of the ore bodies in the Hedong section.

6.5.4 Anomalous zones and exploration directions

On the basis of the element combination anomaly characteristics at different levels, the YC-3 and YC-8 anomalous zones in the Hedong mining section show a high degree of overlap with the I-6 ore body. In the YC-4 anomalous zone, the deep area where the front halo and tail halo overlap corresponds to the VI-1 ore body. In the Hexi mining section, the YC-1 and YC-5 anomalous zones overlap with the H8 ore body. Within these anomalous zones, the maximum anomalies of the front halo and high anomalies of the tail halo overlap, suggesting significant exploration potential in the deeper parts of YC-1 and YC-5 (Fig. 5).

The element association method has been successfully applied in multiple mining districts in northeastern Yunnan Province. A representative case documented by Han et al. in the Huize Pb–Zn deposit demonstrated that this approach effectively identified concealed ore bodies, resulting in a 2-million-ton increase in Zn–Pb metal reserves (Han et al. 2015). This case study exemplifies the practical significance of structural geochemical approaches in industry–academia research collaboration.

6.6 Latent uncertainties in element association method

The element association method has significant advantages in deep concealed deposit prediction:

(1) Comprehensive characterization of mineralization processes: Metallogenic fluids typically transport multiele-

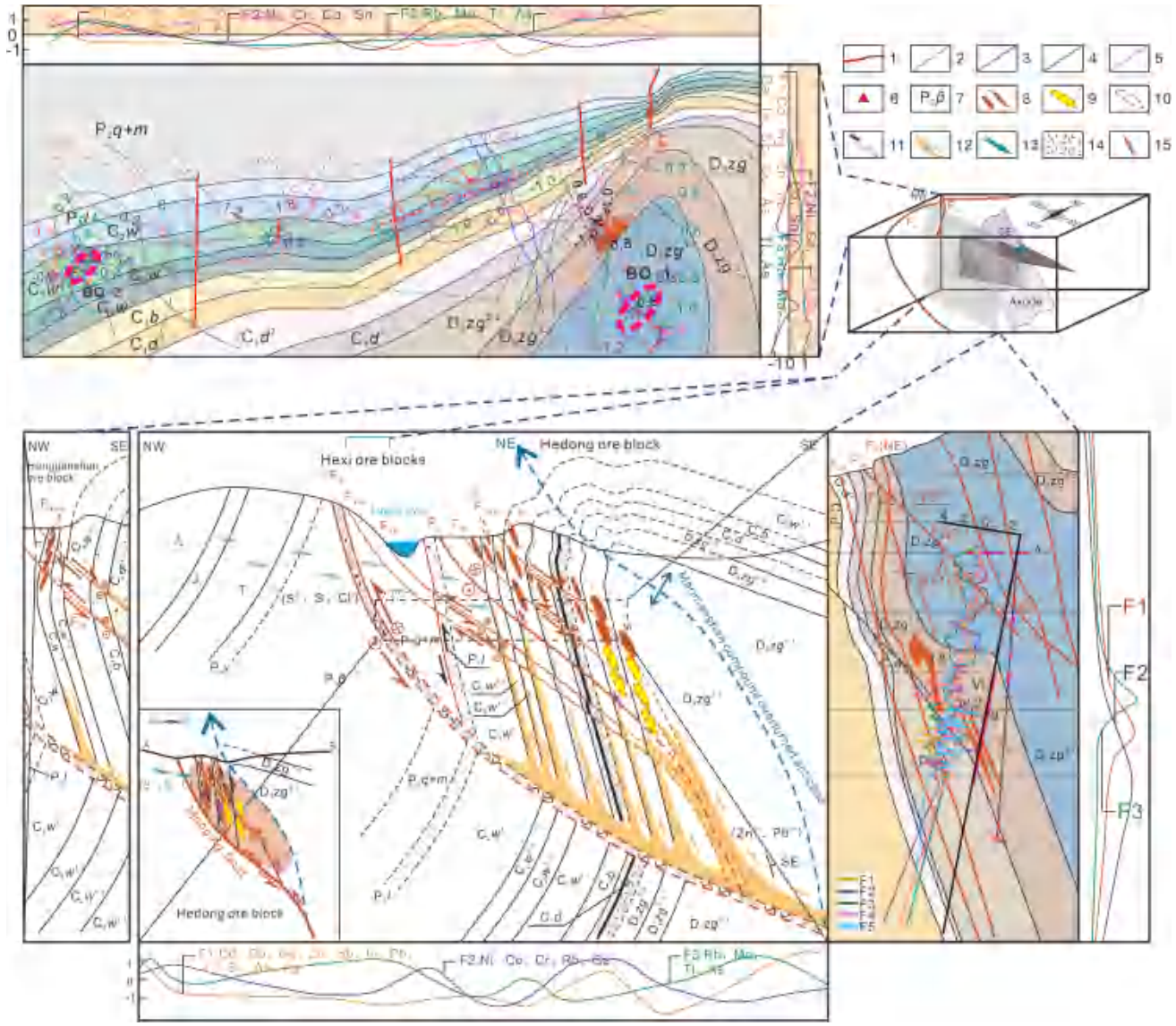

Fig. 15 Deep anomaly model of tectono-geochemical anomalies (Wu et al. 2023; Han et al. 2024). 1. Fault; 2. F1 factor element combination anomaly; 3. F2 factor element combination anomaly; 4. F3 factor element combination anomaly; 5. F4 factor element combination anomaly; 6. Sampling point; 7. Stratigraphy and codes; 8. Known ore body; 9. Predicted ore body; 10. Eroded ore body; 11. Dolomitization and cemented limestone breccia; 12. Ore-forming fluid; 13. Reducing fluid; 14. Argillaceous and sandy clastic rocks; 15. Ore-forming fluid migration direction

ment assemblages (e.g., [Cd-Cu-Ge-Zn-Sb-In-Pb-Sr(-)-As-Hg] in the F1 factor), whose anomaly gradients reflect fluid migration pathways and mineralization centers.

(2) Enhanced anomaly signal-to-noise ratio: Compared with single-element analysis (e.g., Pb, Zn), factor score superposition amplifies weak geochemical signals.

(3) Dynamic zoning interpretation: Vertical zoning patterns of different factor combinations (F1–F4) (Fig. 11) reveal ore body plunge directions and fluid migration mechanisms, providing critical constraints for 3D prospecting models.

Limitations of geochemical element association anomalies:

(1) Structural interference effects:

Lithological–structural complexity may cause mixed anomalies from host rocks, structures, and wall rock alteration. Dynamic threshold adjustment can be implemented to redefine anomaly thresholds; for instance, applying distinct cutoff criteria to factor scores of different element associations improves anomaly accuracy.

Intense silicification or pyritization may amplify As-Sb anomalies that are occasionally unrelated to mineralization, necessitating verification through alteration of mineral assemblages and geological constraints.

(2) Statistical method constraints:

Data distribution assumption: Factor analysis requires normal element distributions, but enrichment-related elements (e.g., Pb and Zn) sometimes exhibit extreme value deviations, compromising factor loading interpretations.

Sampling density limitations: Insufficient/inhomogeneous sampling in challenging terrains may cause localized anomaly omissions. Solutions include sampling density optimization and spatial interpolation algorithm selection.

7 Conclusions

(1) The tectono-geochemical anomaly distribution shows a high degree of overlap with known ore bodies, indicating that anomalies in element combinations (Cd-Cu-Ge-Zn-Sb-In-Pb-Sr(-)-As-Hg; Ni-Co-Cr-Rb-Ga; Rb-Mo-Tl-As; and Ba-Ga) can effectively provide deep exploration information for concealed ore bodies. Moreover, significant differences in the main ore-forming element combinations are observed between the Hedong and Hexi mining sections, with Zn enrichment dominating in Hedong and Pb enrichment dominating in Hexi.

(2) Tectono-geochemical anomalous structure reflects the spatial distribution characteristics of ore bodies and the migration directions of ore-forming fluids. The anomaly gradients of element combinations suggest that concealed ore bodies in the Hedong mining section extend laterally in the NE–SW direction, whereas those in the Hexi mining section extend laterally in the NE–SW direction. The high degree of anomaly overlap among multiple factor element combinations (F2, F3, and F4) near the ore bodies indicates steeply dipping concealed ore bodies. The spatial variation in anomalies further may be two favorable migration directions of ore-forming fluids along fault zones: from the SE at depth to the NW at shallower levels in Hedong and from the SW at depth to the NE at shallower levels in Hexi, ultimately forming deposits.

(3) Directions for deep exploration of the deposit are proposed on the basis of deep evaluation criteria and an exploration model of the tectono-geochemical characteristics of the deposit. This study provides a scientific basis for the deployment of deep mineral exploration and serves as a model for applying tectono-geochemical exploration techniques in the northeastern Yunnan mineralization concentration area.

Acknowledgements This work was financed jointly by National Natural Science Foundation of China (42472127, 42172086), Yunnan Major Science and Technological Projects (202202AG050014), the Yunnan Major Project of Basic Research (202401BN070001-002), Yunnan Mineral Resources Prediction and Evaluation Engineering Research Center (2011), and Yunnan Provincial Geological Process and Mineral Resources Innovation Team (2012).

Author contributions In this paper, the specific contributions of each author are as follows: Conceptualization, Yixuan Yang; Data curation, Hongsheng Gong; Funding acquisition, Runsheng Han and Yan Zhang; Investigation, Yixuan Yang, Jianbiao Wu and Yaya Mi; Methodology, Yixuan Yang and Runsheng Han; Project administration, Runsheng Han; Resources, Gaoming Zhou and Runsheng Han; Software, Yixuan Yang; Validation, Runsheng Han; Visualization, Yixuan Yang; Writing – original draft, Yixuan Yang; Writing – review & editing, Runsheng Han, Yixuan Yang, Yan Zhang, Hongsheng Gong and Jianbiao Wu.

Data availability Data will be made available on request.

Declarations

Conflict of interest On behalf of all authors, the corresponding author states that there is no conflict of interest.

References

Bauer TE, Lynch EP, Sarlus Z, Drejing-Carroll D, Martinsson O, Metzger N, Wanhainen C (2022) Structural controls on iron oxide copper-gold mineralization and related alteration in a Paleoproterozoic supracrustal belt; insights from the Nautanen deformation zone and surroundings, Northern Sweden. Econ Geol 117:327–359. https://doi.org/10.5382/econgeo.4862

Chelle-Michou C, Rottier B, Caricchi L, Simpson G (2017) Tempo of magma degassing and the genesis of porphyry copper deposits. Sci Rep 7:40566. https://doi.org/10.1038/srep40566

Chen YC (1994) Metallogenic series of ore deposits. Earth Sci Front 90–94

Chen S (2014) The study of alteration facies and tectonic-geochemical ore-respecting in Zhaotong lead-zinc deposit. PhD Dissertation, Kunming University of Science and Technology

Cheng Z, Wang Q, Liu J, Pang Z, Yan T, Du Z, Bing M, Yuan H, Lin C (2024) Hidden deposit exploration using the tectono-geochemistry method in the western Xicheng ore field. China China J Geochem Explor 267:107592. https://doi.org/10.1016/j.gexplo.2024.107592

Fan W, Liu G, Chen Q, Lu L, Cui Z, Zuo B, Wu X (2024) Extraction of weak geochemical anomalies based on multiple-point statistics and local singularity analysis. Comput Geosci 28:157–173. https://doi.org/10.1007/s10596-024-10272-3

Fang W (2016) On tectonic system of hydrothermal Breccia: objective, methodology and Lithofacies-mapping applications. Geotecton Metallog 40:237–265

Ghezelbash R, Maghsoudi A, Carranza EJM (2019) Mapping of single- and multi-element geochemical indicators based on catchment basin analysis: application of fractal method and unsupervised clustering models. J Geochem Explor 199:90–104. https://doi.org/10.1016/j.gexplo.2019.01.017

Gong H, Han R, Wu P, Chen G, Li L (2021) Constraints of S-Pb–Sr Isotope Compositions and Rb–Sr Isotopic Age on the Origin of

the Laoyingqing Noncarbonate-Hosted Pb–Zn Deposit in the Kunyang Group, SW China. Geofluids 2021:1–21. https://doi.org/10.1155/2021/8844312
Han RS (2003) Preliminary discussion on research contents and methods of tectono-metallogenic dynamics and concealed ore orientation prognosis. Geol Prospect 39:5–9
Han R (2005) Ore field (bed) tectono-geochemical method for location prediction of concealed ore deposits. Geol Bull China Z1:104–110
Han R (2013) Main study progress for ten years of tectono-geochemistry. Bull Mineral Petrol Geochem 32:198–203
Han R, Wang F, Zhao G, Wang J, Zhou G, Wang X (2010) New progress in deep prospecting of Zhaotong Maoping lead-zinc deposit in the eastern ore concentration area of northern Yunnan. Earth Sci Front 17:275
Han RS, Chen J, Wang F, Wang XK, Li Y (2015) Analysis of metal–element association halos within fault zones for the exploration of concealed ore-bodies — A case study of the Qilinchang Zn–Pb–(Ag–Ge) deposit in the Huize mine district, northeastern Yunnan, China. J Geochem Explor 159:62–78. https://doi.org/10.1016/j.gexplo.2015.08.006
Han R, Wu P, Wang F, Zhou G, Li W, Qiu W (2019) 'Four steps type' ore-prospecting method for deeply concealed hydrothermal ore deposits: a case study of the Maoping Zn-Pb-(Ag-Ge) deposit in southwestern China. Geotecton Met 43:246–257
Han R, Zhang Y, Ren T, Qiu W, Wei P (2020) A summary of research on carbonate-hosted, non-magmatic, epigenetic, hydrothermal type Pb-Zn deposits. J Kunming Uni Sci Tech 45:29–40
Han R, Wu P, Zhang Y, Huang Z, Wang F, Jin Z, Zhou G, Shi Z, Zhang C (2022) New research progress in metallogenic theory for rich Zn-Pb-(Ag-Ge) deposits in the Sichuan-Yunnan-Guizhou Triangle (SYGT) area, southwestern Tethys. Acta Geol Sin 96:554–573
Han R, Wu J, Zhang Y, Chen Q, Sun B (2024) Oblique distribution patterns and the underlying mechanical model of orebody groups controlled by structures at different scales. Sci Rep 14:4591. https://doi.org/10.1038/s41598-024-55473-z
Ji P (2019) Analysis of geochemical characteristics and ore-controlling factors of Maoping lead-zinc deposit in Yiliang County. Chengdu University Of Technology, Yunnan Province
Kaiser HF (1974) A note on the equamax criterion. Multivar Behav Res 9:501–503. https://doi.org/10.1207/s15327906mbr0904_9
Li X (2022) Vertical variation law of physical and chemical conditions of ore-forming fluid in Maoping germanium-rich lead-zinc deposit, northeastern Yunnan. Kunming University of Science and Technology
Men G (1979) Preliminary application of factor analysis. Coal Geol Explor 7:6–12
Qiu L, Yan DP, Yang WX, Wang J, Tang X, Ariser S (2017) Early to Middle Triassic sedimentary records in the Youjiang Basin, South China: implications for Indosinian orogenesis. J Asian Earth Sci 141:125–139. https://doi.org/10.1016/j.jseaes.2016.09.020
Shen Z, Jin C, Dai Y, Yu Z, Hai Z (2016) Mineralization age of the maoping Pb-Zn deposit in the Northeastern Yunnan province: evidence from Rb-Sr isotopic dating of sphalerites. Geol J China Univ 22:213–218
Speczik S, Zieliński K, Bieńko T, Pietrzela A (2021) The prospecting strategy for a deep Cu-Ag ore deposit in Poland – An anatomy of success. Ore Geol Rev 131:104053. https://doi.org/10.1016/j.oregeorev.2021.104053
Sun JC, Han RS (2015) Theory and Methods of Geomechanics in Ore Fields. Science Press, Beijing
Tu G (1984) Tectonics and Geochemistry. Geotecton Metallog 8:1–5
Wan X, Han R, Li B, Xiao X, He Z, Wang J, Wei Q (2022) Tectono-geochemistry and deep prospecting prediction in the Lekai lead-zinc deposit, Northwestern Guizhou Province, China. Geology in China 49:1875–1892
Wang M, Han R, Wang L, Liu F, Guo Y, Tan W (2016) Tectono-geochemical characteristics of Wandongshan-Bijiashan ore block in the Beiya Au-polymetallic deposit, northwestern Yunnan. Geol China 43:238–248
Wang Q, Wang X, Liu H, Tian M, Zhang B, Li R, Yang D, Xiong Y (2021) Targeting deep-seated gold deposits: a study from the qujia gold deposit, Shandong province. China Appl Geochem 130:104982. https://doi.org/10.1016/j.apgeochem.2021.104982
Wang SC, Xu YG, Hou HQ (1992) The basic ideas and methods of comprehensive information metallogenic series prediction. Chin Geol :12–14
Wang X (2010) Study on the application of tectonic geochemical prospecting in Hedong area of Maoping lead-zinc mine in Yiliang, Zhaotong. Master's thesis, Kunming University of Science and Technology
Wu J, Han R, Zhou G, Shi Z, Zhang Y, Sun B, Zhong H, Liu X, Zuo J (2023) Structural ore-controlling and deep prospecting direction of the Maoping lead-zinc deposit in Northeastern Yunnan, China. Geotecton Metallog 47:984–1001
Wu J, Han R, Zhang Y, Sun B, Li W, Li D, Cao Y, Cen C (2024a) The fault–fold structure ore control mechanism of hydrothermal deposits——A case study of the Maoping super-large rich-Ge lead–zinc deposit in northeastern Yunnan. China Ore Geol Rev 168:106039. https://doi.org/10.1016/j.oregeorev.2024.106039
Wu J, Han R, Zhang Y, Wu P, Gong H, Wang L, Cheng G, Li X, Yang Y, Mi Y (2024b) Porosity–permeability characteristics and mineralization–alteration zones of the Maoping germanium-rich lead–zinc deposit in SW China. Front Earth Sci 12:1347243. https://doi.org/10.3389/feart.2024.1347243
Xiao K, Zhu Y, Song G (2000) GIS quantitative evaluation of mineral resources. Chin Geol :29–32
Xiao K, Ding J, Liu R (2006) The discussion of three-part form of non-fuel mineral resource assessment. Fact Sheet :793–798
Yang Q, Liu W, Zhang J, Wang J, Zhang X (2019) Formation of Pb–Zn deposits in the Sichuan–Yunnan–Guizhou triangle linked to the Youjiang foreland basin: evidence from Rb–Sr age and in situ sulfur isotope analysis of the Maoping Pb–Zn deposit in northeastern Yunnan Province, southeast China. Ore Geol Rev 107:780–800. https://doi.org/10.1016/j.oregeorev.2019.03.022
Yang X, Wu J, Coulson IM, Zhang J, Lai X, Zhang Y, Xu D, Liu J, Li G, Li H (2020) Discovery of concealed ore-bodies at the Dongping gold deposit, northern China, revealed by the study of ore-controlling structures. Ore Geol Rev 118:103216. https://doi.org/10.1016/j.oregeorev.2019.103216
Ye T, Xiao K, Yan G (2007) Methodology of deposit modeling and mineral resource potential assessment using integrated geological information. Earth Sci Front 11–19
Zhai YS (1999) On the metallogenic system. Earth Sci Front 14–28
Zhang C, Manheim FT, Hinde J, Grossman JN (2005) Statistical characterization of a large geochemical database and effect of sample size. Appl Geochem 20:1857–1874. https://doi.org/10.1016/j.apgeochem.2005.06.006
Zhao PD, Chen YQ (1998) The main way of geo-anomaly location of ore body. Earth Sci 23:111–114
Zhao J, Zuo R, Chen S, Kreuzer OP (2015) Application of the tectono-geochemistry method to mineral prospectivity mapping: a case study of the Gaosong tin-polymetallic deposit, Gejiu district, SW China. Ore Geol Rev 71:719–734. https://doi.org/10.1016/j.oregeorev.2014.09.023
Zhao D, Han R, Liu F, Fu Y, Zhang X, Qiu W, Tao Q (2022) Constructing the deep-spreading pattern of tectono-geochemical anomalies and its implications on the Huangshaping W-Sn–Pb–Zn polymetallic deposit in southern Hunan. China Ore Geol Rev 148:105040. https://doi.org/10.1016/j.oregeorev.2022.105040

Zuo RG (2019) Exploration geochemical data mining and weak geochemical anomalies identification. Earth Sci Front 26:67–75. https://doi.org/10.13745/j.esf.sf.2018.6.25